Journal of Molecular Liquids 360 (2022) 119463

Contents lists available at ScienceDirect

Journal of Molecular Liquids

journal homepage: www.elsevier.com/locate/molliq

Multi-component analysis, molecular model construction, and thermodynamics performance prediction on various rejuvenators of aged bitumen

Shisong Ren *, Xueyan Liu, Sandra Erkens, Peng Lin, Yangming Gao

Section of Pavement Engineering, Faculty of Civil Engineering & Geosciences, Delft University of Technology, Stevinweg 1, 2628 CN Delft, The Netherlands

ARTICLE INFO

Article history:
Received 12 April 2022
Revised 17 May 2022
Accepted 23 May 2022
Available online 27 May 2022

Keywords:
Rejuvenators
GC–MS characterization
Multi-component molecular model
Molecular dynamics simulation
Thermodynamics performance

ABSTRACT

The molecular dynamics (MD) simulation method is proved as an efficient tool to explore the intermolecular interaction between rejuvenators and aged bitumen, but the simple "single-molecule" model of rejuvenator would bring the inaccuracy to simulation outputs due to a huge difference with its realistic multi-component chrematistic. This study aims to in-depth analyze the chemical components of four commonly-used rejuvenators with the Gas chromatography-mass spectrometry (GC–MS) method, and propose their multi-component molecular models for the first time. Further, MD simulations are performed on the multi-component models of various rejuvenators to anticipate and compare their atomic-level properties. The GC–MS results reveal that the chemical components of petroleum-based rejuvenators are more complicated than the bio-oil (BO). The alkane, naphthenic, and aromatic molecules are the main constituents of engine-oil (EO), naphthenic-oil (NO), and aromatic-oil (AO) rejuvenators. The experimental density results validate the reliability of these multi-component molecular models of four rejuvenators. From the MD simulations outputs, there is a significant difference in the energetic indices, cohesive energy density (CED), solubility parameter δ, volumetric parameters, dynamic behaviors, structural indicators, expansion coefficient (α and β), and isobaric heat capacity (C_p) between the multi-component models of four rejuvenators. However, the multi-component molecular model of aromatic-oil based on the GC–MS method is not accurate because the polycyclic aromatic molecules with heavy-weight are not detected and considered. This study detects the difference in chemical components and thermodynamics properties between four rejuvenators and proposes their more realistic multi-component molecular models for further MD simulations on the rejuvenation of aged bitumen.

1. Introduction

As the service life of asphalt roads prolongs, the bitumen binder is aged because of the thermal oxidation, leading to the increment in its cracking and moisture damage potential [1–3]. During the aging of bitumen, the light-weight oily fractions (saturates and aromatics) converse into the heavy molecules (resins and asphaltenes) [4,5]. Moreover, the oxidation reactions incorporate the polar oxygen-containing functional groups in bitumen molecules, such as the carbonyl and sulfoxide groups [6–8]. However, the aging mechanism of bitumen is complex and still not clear, which strongly depends on several factors of bitumen components, temperature, pressure, and moisture [9–12].

To achieve the goal of sustainable asphalt pavement, the reuse of reclaimed asphalt pavement (RAP) waste materials attracts more attention but it is challenging due to the high stiffness, cracking potential, and moisture sensitivity [13–15]. To supplement the lost lightweight fractions in aged bitumen after aging and dissolve the increased heavy-weight molecules, the oily products (named rejuvenators or recycling agents) are always incorporated in aged bitumen to reactivate its mechanical performance. Different kinds of rejuvenators from bioresources (such as vegetable oils [16], waste cooking oils [17], and other bio-oils [18]) and petroleum-based products (like engine oils [19], naphthenic oils [20], aromatic oils [21], etc.) have been proved to be efficient in improving the low-temperature cracking resistance, fatigue life, workability, and durability of aged bitumen and mixture [22,23]. It is consensus that the rejuvenation efficiency and mechanism of rejuvenators on chemical, physical and mechanical properties of aged bitumen significantly depend on the rejuvenator types and components

* Corresponding author.
E-mail address: Shisong.Ren@tudelft.nl (S. Ren).

https://doi.org/10.1016/j.molliq.2022.119463
0167-7322/

[24,25]. It brings the difficulty to select an optimum rejuvenator for one specific aged bitumen, and explore the underlying interaction mechanisms between aged bitumen with various rejuvenators. Therefore, it is of great importance to make a classification list of various rejuvenators. Unfortunately, there is still no uniform standard for the rejuvenator selection, and most cases are based on experience or existing materials.

Apart from the viscosity-based standard [26], the America National Center for Asphalt Technology (NCAT) summarizes these rejuvenators into five categories of paraffinic oils, aromatic extracts, naphthenic oils, triglycerides & fatty acids, and tall oils based on the difference in material source and chemical compositions of these rejuvenators [27,28]. The examples and descriptions of rejuvenators in each group are summarized in Table 1. The paraffinic oils, aromatic extracts, and naphthenic oils are the byproducts of petroleum processing, while the triglycerides (fatty acids) and tall oils are both bio-based materials [29]. Generally, the chemical components of crude oil are complicated and strongly depend on the source. Based on the molecular distribution, crude oil is always divided into the paraffinic, intermediate, and cycloalkyl groups [30]. Similarly, the chemical compositions in paraffinic oils, aromatic extracts, and naphthenic oils are significantly different [31]. The main components in paraffinic oils, like engine oil or lubricating oils, are the saturated long-chain alkane molecules, while the rejuvenators in the aromatic extracts group are rich in aromatic hydrocarbons [28]. Moreover, more naphthene molecules with saturated aromatic rings are found in naphthenic oils [32]. On the other hand, the triglycerides and fatty acids molecules are the main components in vegetable and cooking oils [33]. Lastly, tall oils are the by-products of the paper industry, and it is separated from other bio-oils because there are lots of polar oxygen-containing functional groups in their molecular structures [29].

However, it is impossible to fully distinguish the difference in rejuvenation efficiency and mechanism between these rejuvenator groups through laboratory tests. The molecular dynamics simulation is an efficient method, and it has been successfully utilized in rejuvenated bitumen systems [34,35]. The rejuvenation efficiency of rejuvenators could be evaluated through the thermodynamics properties predicted from MD simulations, such as the cohesive energy density, solubility parameter, surface free energy, work of cohesion, viscosity, and glass transition temperature, and colloidal structure [36–40]. Previous studies also investigated the diffusion behaviors and blending degree of rejuvenators in aged bitumen with MD simulations [41–43]. To ensure the reasonability of MD simulation outputs, the molecular structures of rejuvenators should be more accurate. Nevertheless, it is found that the molecular structures of the rejuvenator in all MD simulation cases are the average model, in which only a sort of molecule is employed to represent the whole rejuvenator [41–43]. It is conflicting with the actual situation that the rejuvenators (especially petroleum-based) are complicated with numerous kinds of molecules. Thus, the simplification of rejuvenator components into one type of molecule would result in a huge difference between the MD simulation outputs and experimental results. In addition, it should be mentioned that the lack of in-depth chemical component characterizations and analysis also restricts the development of precise molecular models of rejuvenators.

Table 1
Classifications of different typical rejuvenators for aged bitumen recycling [27,28].

Category	Examples	Description
Paraffinic oils	Waste engine oil or waste engine oil bottom	Refined used lubricating oils
Aromatic extracts	Commercial products	Refined crude oil products with polar aromatic oil components
Naphthenic oils	Commercial products	Engineered hydrocarbons for asphalt modification
Triglycerides & fatty acids	Waste vegetable oil Oleic acid	Derived from vegetable oils
Tall oils	Commercial products	Paper industry by-products; Same chemical family as liquid anti-strip agents and emulsifiers

The objective of this study was to analyze the chemical components in various commonly-used rejuvenators of aged bitumen. Meanwhile, the multi-component molecular models of rejuvenators were established as the essential inputs for molecular dynamics (MD) simulations, which could help us fully understand the difference in chemical, physical and thermodynamics properties between different kinds of rejuvenators. Fig. 1 illustrates the main flow chart of this research. Four types of rejuvenators were selected in this study, including the bio-oil, engine-oil, naphthenic-oil, and aromatic-oil. The gas chromatography-mass spectrometry (GC–MS) method was conducted to detect the chemical components and molecules in various rejuvenators. Based on the GC–MS results, the main constituents were chosen to build the multi-component molecular models of rejuvenators, which were then subjected to MD simulations to further predict and compare the nanoscale thermodynamics performance of different rejuvenators in terms of energetic parameters, cohesive energy density, solubility parameter, volumetric indices, dynamics behaviors and structural characteristics.

2. Rejuvenators and GCMS method

2.1. Rejuvenators

A wide variety of rejuvenators have been developed and utilized to reactivate and improve the chemical and rheological properties of aged bitumen [28,44,45]. To basically and comprehensively understand the chemical components of rejuvenators, four widely-utilized rejuvenators, including bio-oil (BO), engine-oil (EO), naphthenic-oil (NO), and aromatic-oil (AO), were chosen and tested. All rejuvenators used in this study are purchased from the market. Table 2 displays the physical and chemical properties of these four rejuvenators. The aromatic-oil rejuvenator shows the highest density, viscosity, C%, and molecular weight. Meanwhile, the bio-oil rejuvenator exhibits the largest O% due to the existence of the ester functional group. Besides, the magnitude order of molecular weight and viscosity for four rejuvenators is BO < EO < NO < AO, while the sequence of density presents as EO < NO < BO < AO.

2.2. GC–MS method

In this study, the chemical components in various rejuvenators were identified using the GC–MS test, which was an efficient way to analyze tiny amounts of a substance. Previous work also successfully detected the chemical compositions in bio-based rejuvenators [22,23]. The basic working principle of the GC–MS method is drawn in Fig. 2. The rejuvenator molecules are retained by the column and eluted from the column at different times (retention time) due to the difference in polarity and solubility [46]. Afterward, the separated molecules are captured, ionized, accelerated, and detected by a mass spectrometer through the measurement of molecule mass. The GC–MS used was Agilent 6890 N/5975 from the USA. About 1 mg of rejuvenator sample was purged with inert gas (Nitrogen) into an airtight chamber at room temperature. The pyrolysis temperature and time were 200 °C and 15 s with an

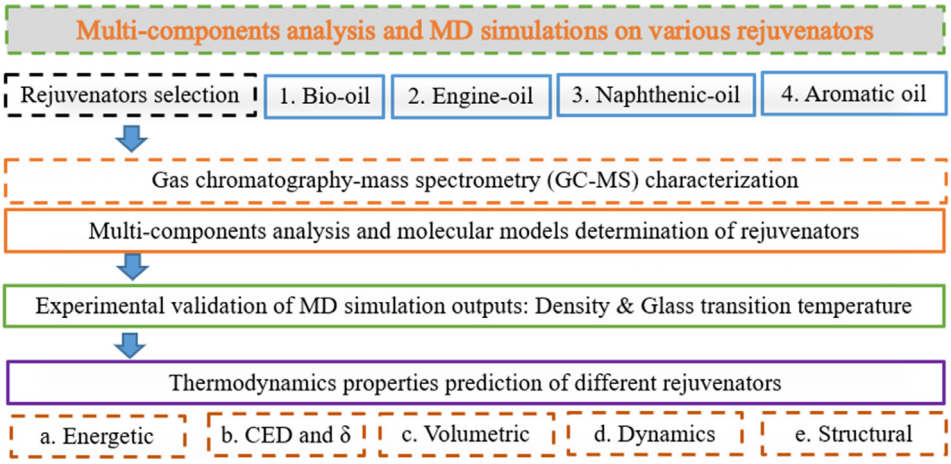

Fig. 1. Scheme illustration of research methodologies.

Table 2
Chemical and physical properties of rejuvenators.

Rejuvenators	Bio-oil	Engine-oil	Naphthenic-oil	Aromatic-oil
Appearance	Pale-yellow liquid	Brown liquid	Transparent-liquid	Dark-brown half-solid
25℃ Density (g/cm^3)	0.911	0.833	0.875	0.994
60℃ Density (g/cm^3)	0.899	0.814	0.852	0.978
25℃ viscosity (cP)	50	60	130	63,100
Flash point (℃)	> 250	> 225	> 230	> 210
Carbon C (%)	76.47	85.16	86.24	88.01
Hydrogen H (%)	11.96	14.36	13.62	10.56
Oxygen O (%)	11.36	0.12	0.10	0.40
Sulfur S (%)	0.06	0.13	0.10	0.48
Nitrogen N (%)	0.15	0.23	0.12	0.55
Mn (g/mol)	286.43	316.48	357.06	409.99

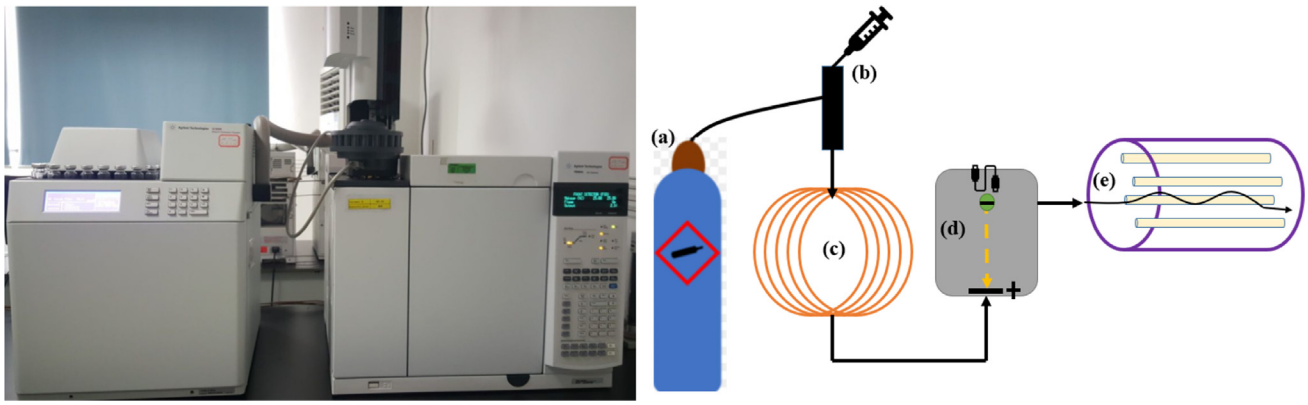

Fig. 2. The basic working principle of the GC–MS method (a) Inert gas system; (b) injector; (c) gas chromatography column; (d) ionization room; (e) a mass spectrometry measurement system.

increasing rate of 10 °C/ms [47]. Besides, the electron energy and scanning range applied to the system was selected as 70 eV and 30–1000 amu., respectively. Lastly, the type and amount of substances in each rejuvenator were outputted from the GC–MS curve.

3. GC–MS results and discussion

The gasoline and diesel oil both contain several types of alkanes with different carbon-chain lengths. Similarly, the generic rejuvenators from petroleum products are complicated and composed of numerous molecules. To understand the difference in rejuvenation efficiency and mechanism between these rejuvenators at the nanoscale, the chemical characterizations and representative molecular models' establishment of rejuvenators are of great significance. In this study, the molecular compositions of rejuvenators are detected through the GCMS method, and the corresponding results are shown and discussed herein.

3.1. Chemical components in bio-oil rejuvenator

Fig. 3 displays the GCMS result of the bio-oil rejuvenator, and six characteristic peaks of chemical molecules with the retention

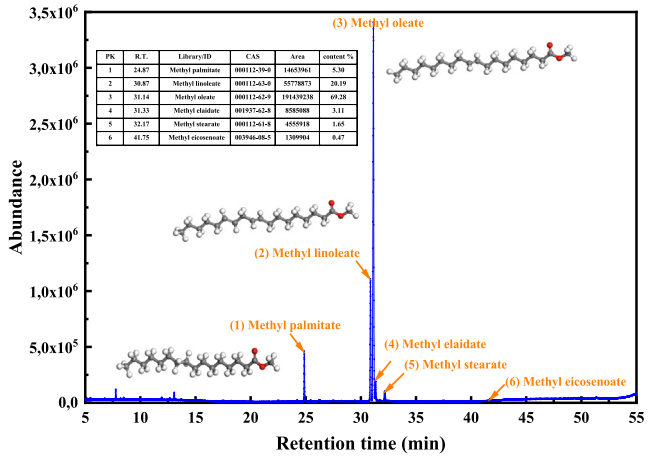

PK	R.T.	Library/ID	CAS	Area	content %
1	24.87	Methyl palmitate	000112-39-0	14653961	5.30
2	30.87	Methyl linoleate	000112-63-0	55778873	20.19
3	31.14	Methyl oleate	000112-62-9	191439238	69.28
4	31.33	Methyl elaidate	001937-62-8	8585088	3.11
5	32.17	Methyl stearate	000112-61-8	4555918	1.65
6	41.75	Methyl eicosenoate	003946-08-5	1309904	0.47

Fig. 3. The GC–MS curve of bio-oil rejuvenator.

time of 24.87, 30.87, 31.14, 31.33, 32.17, and 41.75 min are observed. On basis of the chemical library, these molecules are recognized as methyl palmitate, methyl linoleate, methyl oleate, methyl elaidate, methyl stearate, and methyl eicosenoate. It can be found that oxygen-containing functional groups exist in all molecules of bio-oil, which is consistent with the literature report [22–23]. According to the peak area, the mass fraction of each component is calculated and listed in Table 3**.** The methyl oleate shows the maximum content of 69.28%, followed by the methyl linoleate (20.19%) and methyl palmitate (5.30%), while the mass fractions of the other three molecules are lower than 5.0%. Hence, it is concluded that the bio-oil rejuvenator is mainly composed of methyl oleate, methyl linoleate, and methyl palmitate. Their related molecular structures are also drawn in Fig. 3. It is worth mentioning that the functional group in these three main molecules of bio-oil rejuvenator is identical, while the differences exist in the numbers of the carbon atom and unsaturated double bond C = C in the body chain.

3.2. Chemical components in engine-oil rejuvenator

Apart from the bio-oil, the other three kinds of rejuvenators all come from petroleum refinery processing. As mentioned before, engine oil, naphthenic oil, and aromatic oil rejuvenators are compounds of numerous molecules. Fig. 4a illustrates the GC–MS curve of the engine-oil rejuvenator. Meanwhile, the detailed chemical components in engine-oil are summarized in **Table S1**, which indicates that the engine-oil rejuvenators contain 56 kinds of different molecules approximately. It increases the difficulty to distinguish these components in terms of rejuvenation efficiency and mechanism on aged bitumen. Herein, various molecules in engine-oil rejuvenators are divided into four groups (alkane, monocyclic alkane, olefin, and other additives), according to the separation principle of bitumen into SARA fractions [34].

Fig. 4b shows the dosage of chemical component groups in engine-oil rejuvenator. The alkane molecules present a percentage of 61.79%, which are the main components in engine-oil. Meanwhile, there are about 5.71% monocyclic alkanes and 3.76% olefins, respectively. It should be mentioned that during the production of engine oil, lots of additives were incorporated to improve its application performance, such as anti-aging and lubricity [29]. These additives molecules in engine-oil still occupy the distinct proportion of 28.74%, which should be considered during the determination of the multi-component molecular model for engine-oil rejuvenator. Regarding the alkane group with maximum dosage, Fig. 4c displays the alkane molecules' classification and distribution based on the carbon number in the main chain. It can be found that the alkanes molecules in engine-oil show the various carbon-chain structure, which is determined by petroleum resources and the atmospheric distillation process [18]. Moreover, the carbon numbers in molecular structures of most alkanes are located in the region of 11–20. In detail, the percentage of alkanes with carbon numbers lower than 10, 11–15, 16–20, and higher than 20 is 4.0%, 27.1%, 24.5%, and 6.2%, respectively. From the GC–MS curve, the proportions of several molecules are more apparent, and the corresponding molecular structures are also marked in Fig. 4a**.** The dominant molecules in alkanes are dodecane, tetradecane, hexadecane, octadecane, nonadecane and eicosane. Further, the peak abundance of octadecane is the strongest, followed by the dodecane and 1-methyl-2-pentyl cyclohexane, and the additive molecule of 2,6-bis (1,1-dimethylethyl)-phenol also shows an obvious peak.

3.3. Chemical components in naphthenic-oil rejuvenator

Fig. 5 demonstrates the GC–MS curve of the naphthenic-oil rejuvenator, and it denotes that almost 40 types of molecules exist in naphthenic-oil. The detailed information on all molecules is listed in **Table S2**. These chemical components in naphthenic oil can be divided into three groups, which are alkane, naphthenic, and other hydrocarbons (additives). It should be mentioned that the additive group contains these molecules not belonging to the alkane and naphthenic catalogs. The proportion of alkanes in the naphthenic-oil rejuvenator is approximately 17.85%, while the naphthenic concentration shows a maximum value of 59.79%. Therefore, the main components in the naphthenic-oil rejuvenator are naphthenic molecules, followed by the alkane molecules. Similar to the engine-oil, other impurities molecules are observed in the naphthenic-oil, which comes from different additives during the petroleum processing to enhance the oxidative aging resistance of the naphthenic-oil [24,28]. Due to the complexity and diversity, only main additive molecules are considered to establish the multi-component molecular models of naphthenic-oil as well as engine-oil and aromatic-oil rejuvenators.

For further summarization and analysis, the alkanes and naphthenic molecules are further classified into several groups based on the carbon number in the alkane chain and the number of naphthenic rings in molecular structures, respectively. The corresponding results are shown in Fig. 5c and d. There are several kinds of

Table 3
The main chemical components in bio-oil.

No.	Retention time	Components	CAS	Mass fraction (wt%)
1	24.868	Methyl Palmitate	000112–39-0	5.30
2	30.8748	Methyl Linoleate	000112–63-0	20.19
3	31.1434	Methyl Oleate	000112–62-9	69.28
4	31.332	Methyl Elaidate	001937–62-8	3.11
5	32.1721	Methyl Stearate	000112–61-8	1.65
6	41.7453	Methyl Eicosenoate	003946–08-5	0.47

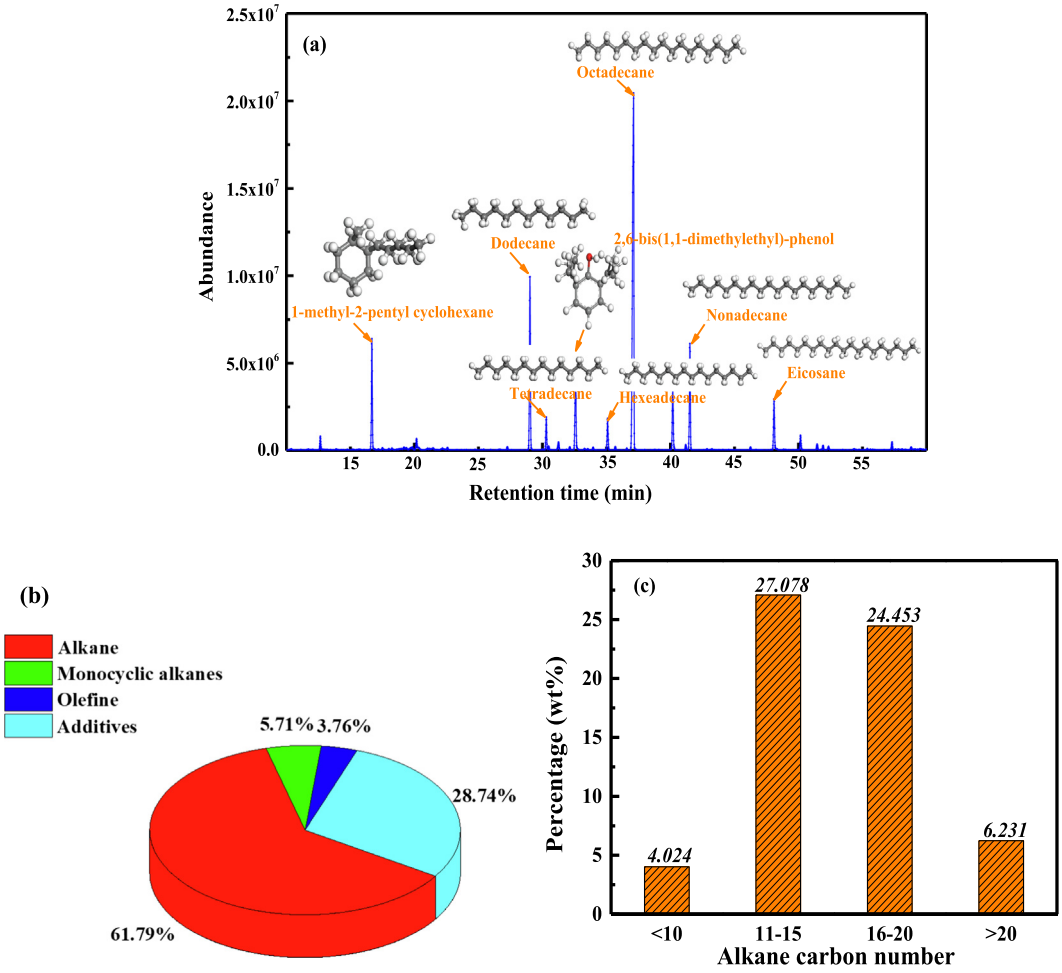

Fig. 4. The components distribution and alkane classification in engine-oil.

alkane molecules with variable carbon-atom numbers in the body chain observed in naphthenic-oil. The carbon number of most alkanes is lower than 20, and the related percentage is 15.76% for all molecules in the naphthenic-oil rejuvenator. In addition, the alkanes concentrations with the chain carbon number of < 10 and 11–15 are both about 4%, while the alkanes proportion with the carbon number of 16–20 is 7.57%. Compared to the engine-oil, the alkane dosage in the naphthenic-oil rejuvenator is significantly lower, while the concentration of naphthenic molecules is much higher.

In addition, the naphthenic molecules in naphthenic-oil are not consistent with the number of naphthenic rings differing from 1 to 4. According to the variable number of naphthenic rings, these naphthenic molecules are divided into four types, including the cyclohexane-based, naphthalene-based, anthracene-based, and pyrene-based molecules. It can be found that the pyrene-based naphthenic molecules show the largest proportion of 29.69%, followed by the anthracene-based (17.01%) and naphthalene-based (11.13%) naphthenic molecules, while the dosage of a cyclohexane-based naphthenic molecule is the lowest of 1.97%. From the GC–MS curve, some molecules with significant dosage show larger peaks than others, which are detected as the 2,3-dimethyl-decahydro-naphthalene, 2-(1-methyl-2-butenyl)-4-methoxy-phenol, hexadcahydro-pyrene, 2,6,10,14-tetramethyl-hexadecane, and heneicosane. Their molecular structures are also displayed in Fig. 5a. The hexadcahydro-pyrene molecule shows the strongest peak value, followed by the 2-(1-methyl-2-butenyl)-4-methoxy-phenol and 2,6,10,14-tetramethyl-hexadecane. At the same time, the molecular concentrations of 2,3-dimethyl-decahydro-naphthene and heneicosane are similar but much lower than the other three molecules.

3.4. Chemical components in aromatic-oil rejuvenator

Fig. 6a illustrates the GC–MS result of the aromatic-oil rejuvenator. Numerous peaks are observed and it proves that the aromatic-oil is a complicated material containing various types of molecules. The detailed chemical components in aromatic-oil are summarized in **Table S3,** and they are categorized into four groups (alkane, olefin, aromatics, and additives). The dosage of these four groups of molecules is presented in Fig. 6b. It is found that the aromatic-oil is mainly composed of alkane, olefin, aromatic molecules as well as other hydrocarbons. The alkane content (13.74%) in aromatic-oil is markedly lower than that in the aforementioned engine-oil (61.79%) and naphthenic-oil (17.85%). However, the concentration of aromatics molecules in aromatic-oil is significant at 53.91%, which is hardly detected in the other three rejuvenators. Moreover, there are about 2.16% of olefins molecules and 30.19% of other hydrocarbons monitored in the aromatic-oil rejuvenator.

The alkanes molecules are distinguished based on the carbon atom number in the body chain of molecular structure, and the results are displayed in Fig. 6c. It is illustrated that the carbon atom number in most alkanes' molecules is located in a region of 11–20, while only 0.27% and 2.05% of alkanes molecules show the carbon atom number lower than 10 and higher than 20, respectively. Moreover, the dosage of alkanes with a carbon atom number of 16–20 is almost 3.5 times than total concentration of alkanes from

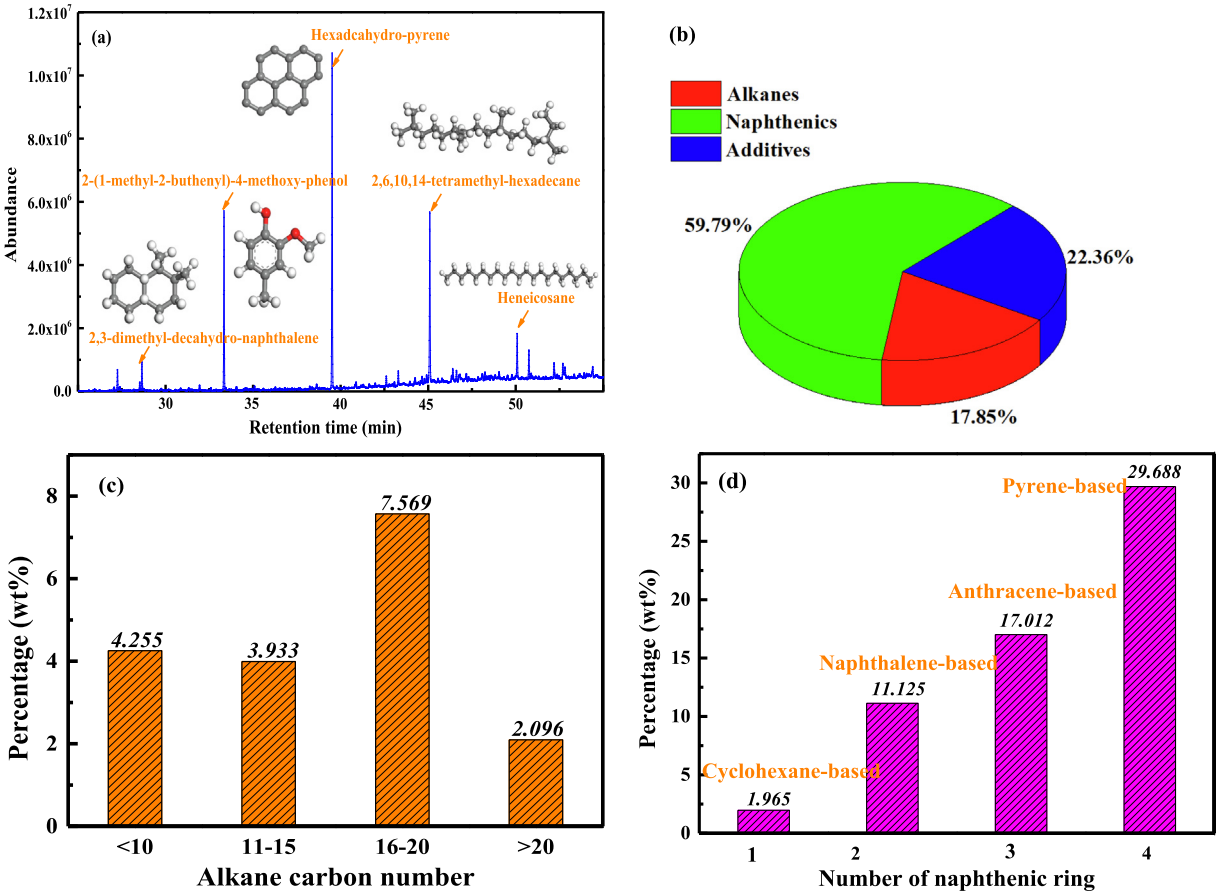

Fig. 5. The components distribution, alkanes, and naphthenic classification in naphthenic-oil.

undecane to pentadecane. On the other hand, the type of aromatics molecules in aromatic-oil is not consistent. In this study, these aromatics molecules are assorted following the number of aromatic rings in their molecular structures, including the benzene-based (single-ring), naphthalene-based (double-rings), and fluorene/indene (multi-rings). The concentration of each aromatics molecular group is shown in Fig. 6d. It can be found that most aromatics molecules are naphthalene-based with a high dosage of 46.73%, while benzene-based and fluorene/indene only accounts for 0.86% and 6.31%, respectively. In the meantime, the naphthalene-based aromatics molecules are classified into five items based on the difference in the number of methyl substituents on aromatic rings, which varies from 0 to 4. Thence, the five groups of naphthalene-based aromatics molecules are named naphthalene, methyl-naphthalene, dimethyl-naphthalene, trimethyl-naphthalene, and tetramethyl-naphthalene. The dosage of naphthalene molecules is the lowest at 1.70%, indicating that the naphthalene molecules in aromatic-oil almost all have the substituents more or less. Interestingly, the concentration of naphthalene-based molecules as the function of methyl substituents amount presents the Gaussian distribution. The methyl-naphthalene and tetramethyl-naphthalene molecules are 6.4% and 5.6%, respectively. In addition, dimethyl-naphthalene and trimethyl-naphthalene show a large dosage of 18.1% and 14.9%. Thus, about 33% of naphthalene-based aromatic molecules present 2 or 3 methyl substituents. It provides the data basis for determining the molecular components of a multi-component molecular model of aromatic-oil rejuvenator.

From the GC–MS curve, the dosage of each molecule in the aromatic-oil rejuvenator is obtained and the main components with apparently large content can be detected. There are six strong peaks detected in the GC–MS curve of the aromatic-oil, and the related molecular structures are also shown in Fig. 6a. As the retention time prolongs, these six chemical components in order are furfural, 5-methyl-2-furfural, naphthalene, 2,7-dimethyl naphthalene, 1,4,6-trimethyl naphthalene, and octadecane. It further validates that the aromatic-oil rejuvenator is mainly composed of alkenes, aromatics, and additives (solvents) molecules. The furfural and 5-methyl-2-furfural are the solvents used during the extraction process of aromatic oils. Moreover, the naphthalene, 2,7-dimethyl naphthalene, and 1,4,6-trimethyl naphthalene molecules are the mainly monitored chemical components in aromatic-oil. In addition, the octadecane denotes the existence of alkanes molecules in an aromatic-oil rejuvenator. In the following section, some of these main components will be selected to represent the different molecular groups to build the multi-component molecular model of aromatic-oil rejuvenator.

4. Molecular determination for multi-component molecular models of rejuvenators

The chemical components distribution in four rejuvenators was detected and analyzed using the GC–MS method in terms of the main molecular groups and molecules with high dosage. However, the molecular components in all rejuvenators are complex and diverse, especially the petroleum-based ones (engine-oil, naphthenic-oil, and aromatic-oil). It significantly brings huge difficulties to find and establish the representative molecular models of these rejuvenators. Besides, it is unrealistic to consider all mole-

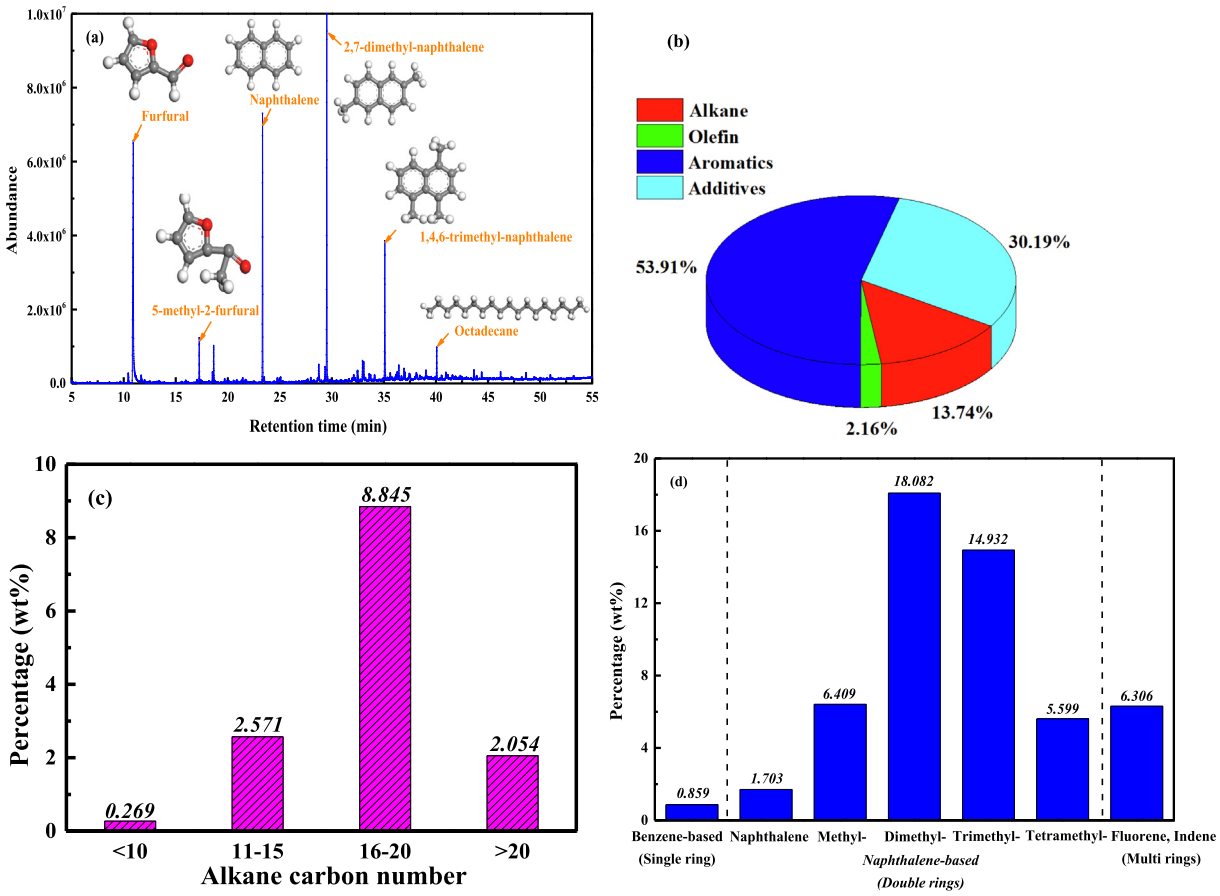

Fig. 6. The components distribution, alkanes, and aromatics classification in aromatic-oil.

cules in building the multi-component molecular models of pure rejuvenators as well as rejuvenated bitumen. It is found that there are 3 or 4 molecular groups containing these petroleum-based rejuvenators, while only 6 kinds of molecules are included in bio-oil rejuvenator. Generally, the molecules representing the saturate, aromatic, resin, and asphaltene fractions are selected to establish the multi-component molecular model of bitumen. Therefore, 3–5 molecules with high dosage in the GC–MS curve are chosen to represent the main chemical molecular groups and establish the representative multi-component molecular models of four rejuvenators.

4.1. Bio-oil rejuvenator

From the GC–MS results, the sum content of methyl palmitate, methyl linoleate, and methyl oleate is 94.77%, and methyl oleate has the highest dosage of 69.28%. Hence, these three molecules are considered to build the multi-component model of bio-oil rejuvenator, and their molecular structures are illustrated in Fig. 7. It can be seen that these three molecules present a similar main-chain structure (aliphatic hydrocarbons) and functional group (ester), and the difference is in the number of carbon atoms and double bonds in the main-chain structure.

In addition, the methyl elaidate (3.1%), methyl stearate (1.7%), and methyl eicosenoate (0.5%) molecules are not considered during the construction of a multi-component model of bio-oil rejuvenator because of their low molecular dosages. Table 4 lists the dosage and the molecular number of these three molecules in the bio-oil rejuvenator. Due to the omission of methyl elaidate, methyl stearate, and methyl eicosenoate molecules, the content of methyl palmitate, methyl linoleate, and methyl oleate in a multi-component model of bio-oil is calibrated as 5.6%, 21.3%, 73.10%, and the corresponding molecular number are 13, 44 and 151, respectively. The model dosage of these three molecules is not completely the same as the real value because the molecular number should be an integer. However, the difference in molecular dosage between calibrated and model values are little at 0.1%. It means that the multi-component model of bio-oil rejuvenator is accurate enough.

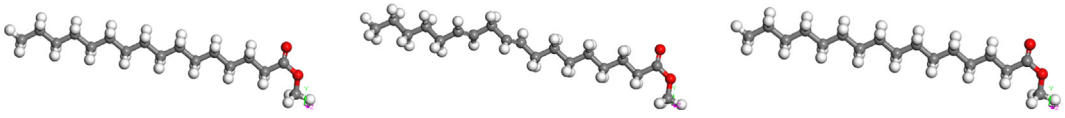

(a) Methyl palmitate (b) Methyl linoleate (c) Methyl oleate

Fig. 7. There molecular elements in the bio-oil rejuvenator.

Table 4
The molecular components in a multi-component molecular model of bio-oil.

No	Components	Measured dosage (wt%)	Calibrated dosage (wt%)	Chemical formula	Molecular number	Model dosage (wt%)
1	Methyl Palmitate	5.30	5.60	$C_{17}H_{34}O_2$	13	5.70
2	Methyl Linoleate	20.19	21.30	$C_{19}H_{34}O_2$	44	21.20
3	Methyl Oleate	69.28	73.10	$C_{19}H_{36}O_2$	151	73.10

4.2. Engine-oil rejuvenator

It was revealed that the engine-oil rejuvenator is mainly composed of alkanes, monocyclic alkanes, and additives molecules. In this study, the tetradecane molecule is selected to represent the alkanes molecular group, and the 1-methyl-2-pentyl-cyclohexane molecule refers to the monocyclic alkanes. Regarding the additives group, the high dosage of 28.7% demonstrates their key role in determining the chemo-physical and thermodynamics properties of engine-oil rejuvenator. Herein, the additive molecules with a dosage higher than 3% are taken into consideration in the multi-component molecular model of engine-oil rejuvenators. These three additive molecules are 2,6-bis (1,1-dimethylethyl)-phenol, 1-pentanol, and butyl benzoate. Fig. 8 manifests the molecular structures of five molecules in a multi-component model of engine-oil. It is found that all three additive molecules show the oxygen-containing functional groups, such as the phenolic, hydroxy, and ester groups. These additive molecules with polar functional groups were incorporated in engine-oil to enhance its anti-aging and performance stability, which was also detected in previous studies [31,48].

In the multi-component model of engine-oil, five main molecules are included and their measure dosages are summarized in Table 5. It should be mentioned that the measured dosage of tetradecane and 1-methyl-2-pentyl molecule comes from the concentration of alkanes and monocyclic alkanes molecular groups to balance the simplicity and accuracy of the engine-oil molecular model. Meanwhile, most additives molecules with low concentrations are ignored, thus the measured dosages of five molecular elements are calibrated as 67.91%, 6.29%, 13.87%, 8.01%, and 3.92%, respectively. In addition, it should be noted that the total number of molecules in different rejuvenators maintains an approaching level. Accordingly, the molecular number of tetradecane, 1-methyl-2-pentyl-cyclohexane, 2,6-bis(1,1-dimethylethyl)-phenol, 1-pentanol and butyl benzoate molecule is 127, 14, 25, 34 and 8, respectively. Further, the molecular dosages of these five molecules in the model are much close to the calibrated values, showing the multi-component model of engine-oil rejuvenator is representative and reasonable.

4.3. Naphthenic-oil rejuvenator

The molecules in the naphthenic-oil rejuvenator belong to different chemical groups of alkanes, naphthenic and other hydrocarbons. Based on the concentration distribution of various alkanes and naphthenic molecules with different carbon-chain lengths and the number of naphthenic rings, the tetradecane and hexadecahydro pyrene molecule is utilized to represent the molecular group of alkanes and naphthenic, respectively. In addition, the 2-methoxy-4-methyl phenol molecule with high content of 14.49% is selected as the additives molecular group. Fig. 9 shows the molecular structures for three types of molecules in the multi-component molecular model of the naphthenic-oil rejuvenator. Similar to additive molecules in engine-oil, the 2-methoxy-4-methyl phenol molecule has the aromatic ring and oxygen-containing functional groups (phenolic and methoxy), which is to improve the performance stability and aging resistance of the naphthenic-oil rejuvenator.

From Table 6, the measured dosage of tetradecane, hexadecahydro pyrene, and 2-methoxy-4-methyl phenol molecule is 17.85%, 59.79%, and 14.49%, respectively. Meanwhile, about 7.87% of molecules (mainly in the additives group) are not considered in the multi-component molecular model of naphthenic-oil rejuvenator. To eliminate that influence, the molecular number of the tetradecane, hexadecahydro pyrene, and 2-methoxy-4-methyl phenol is determined according to the normalized dosage of 19.37%, 64.90%, and 15.73%, which is 39, 120, and 46, respectively. It can be found the model dosages of these three molecules are similar to the experimental values, which guarantees the efficiency and reliability of predicted thermodynamics properties for a multi-component molecular model of naphthenic-oil rejuvenator outputted from MD simulations at the nanoscale level.

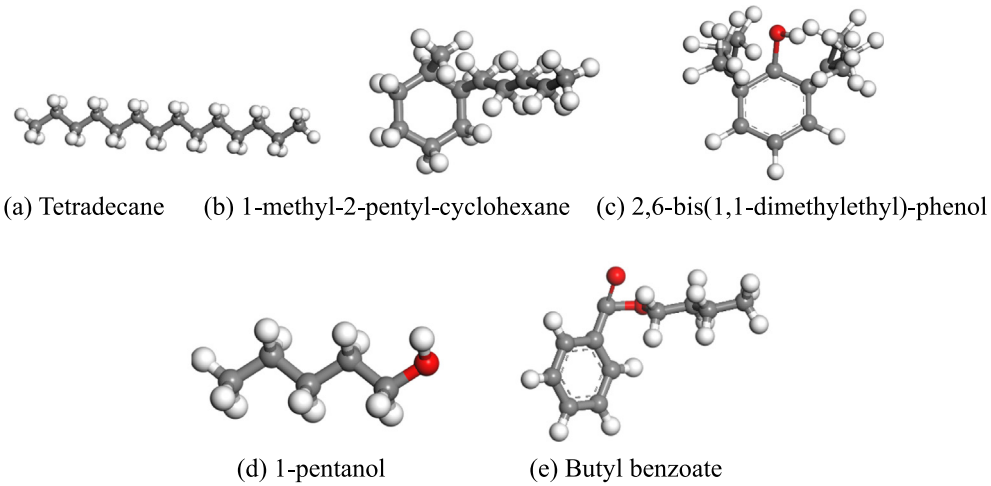

Fig. 8. The molecular elements of engine-oil rejuvenator.

Table 5
The material components in a multi-component molecular model of engine-oil.

No	Components	Measured dosage (wt%)	Calibrated dosage (wt%)	Chemical formula	Molecular Number	Model dosage (wt%)
1	Tetradecane	61.79	67.91	$C_{14}H_{30}$	127	67.9
2	1-methyl-2-pentyl-cyclohexane	5.72	6.29	$C_{12}H_{24}$	14	6.3
3	2,6-bis(1,1-dimethylethyl)-phenol	12.62	13.87	$C_{14}H_{22}O$	25	13.9
4	1-pentanol	7.29	8.01	$C_5H_{12}O$	34	8.1
5	Butyl benzoate	3.57	3.92	$C_{11}H_{14}O_2$	8	3.8

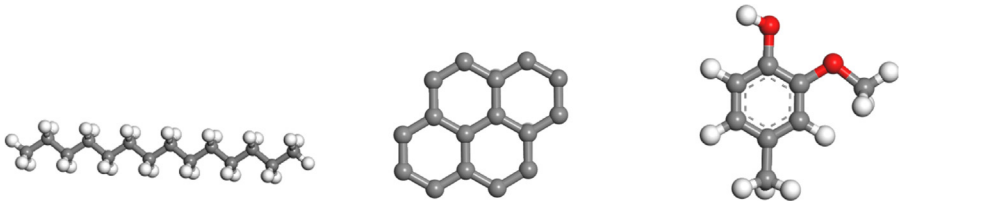

(a) Tetradecane (b) Hexadecahydro pyrene (c) 2-methoxy-4-methyl phenol

Fig. 9. The molecular elements in the naphthenic-oil rejuvenator.

Table 6
The molecular components in naphthenic-oil.

No	Components	Measured dosage (wt%)	Calibrated dosage (wt%)	Chemical formula	Molecular Number	Model dosage (wt%)
1	Tetradecane	17.85	19.37	$C_{14}H_{30}$	39	19.2
2	Hexadecahydro pyrene	59.79	64.90	$C_{16}H_{26}$	120	65.0
3	2-methoxy-4-methyl phenol	14.49	15.73	$C_8H_{10}O_2$	46	15.8

Table 7
The molecular components in aromatic-oil.

No	Components	Measured dosage (wt%)	Calibrated dosage (wt%)	Chemical formula	Molecular number	Model dosage (wt%)
1	Octadecane	13.74	14.65	$C_{18}H_{38}$	22	14.7
2	2,7-Dimethyl Naphthalene	53.91	57.49	$C_{12}H_{12}$	140	57.5
3	Furfural	26.13	27.86	$C_5H_4O_2$	110	27.8

4.4. Aromatic-oil rejuvenator

According to the GCMS result, the aromatic-oil rejuvenator is mainly composed of alkanes, aromatics, and additives (like solvents). In this study, one molecule with maximum dosage in each group is selected to represent the alkanes, aromatics, and solvents molecules, which are the octadecane, 2,7-dimethyl naphthalene, and furfural. Their molecular structures are shown in Fig. 10. Meanwhile, Table 7 lists the measured dosage, calibrated dosage, and chemical formula of these three molecules. The chemical formula of octadecane, 2,7-dimethyl naphthalene, and furfural molecule is $C_{18}H_{38}$, $C_{12}H_{12}$, and $C_5H_4O_2$, respectively. Octadecane is a saturated alkane molecule with an 18-carbons chain, and 13.74% octadecane is detected in aromatic-oil. Moreover, 53.91% 2,7-dimethyl naphthalene is found in aromatic-oil, which contains two aromatic rings connected with counterpoint methyl. About 26.13% of furfural molecules are monitored in the GCMS test of aromatic-oil, which is related to the processing process of aromatic oils with the solvent of furfural [27,49]. To eliminate the influence of other additives molecules, the content of octadecane, 2,7-dimethyl naphthalene, and furfural molecules is calibrated as 14.65%, 57.49%, and 27.86%, respectively. Based on the molecular formula and calibrated dosage, the number of octadecane, 2,7-dimethyl naphthalene, and furfural molecules is determined as 22, 140, and 110. Further, it is found that the dosage of each molecule in the model is close to measured values, and it ensures the reasonability of the multi-component model of aromatic-oil rejuvenator.

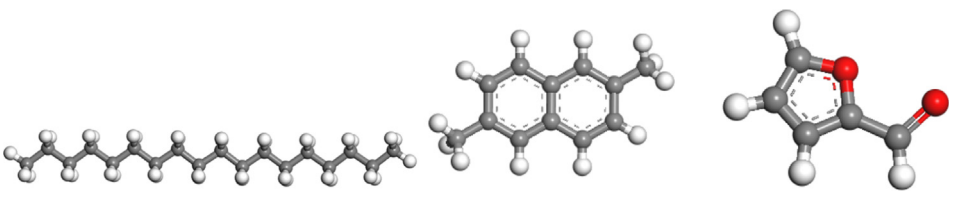

(a) Octadecane (b) 2,7-dimethyl naphthalene (c) Furfural

Fig. 10. The molecular elements in aromatic-oil rejuvenator.

5. Molecular dynamics simulation and validation

The establishment and MD simulations running for multi-component models of four rejuvenators are conducted in Materials Studio 2017 [40–42]. After inputting the molecules in one simulation cubic with an initial density of 0.1 g/cm^3, the molecular models of rejuvenators are subjected to the geometry optimization procedure with periodic boundary conditions to eliminate the atoms overlapping and minimize the total energy of rejuvenator systems. It should be denoted that the COMPASSII force field is utilized throughout the whole MD simulations on multi-component molecular models of all rejuvenators. Afterward, the MD equilibrium simulations with the isothermal-isobaric (NPT, constant atom number, simulation pressure, and temperature) ensemble are implemented on these initial molecular models to achieve the ideal equilibrium molecular models. The adopted pressure and temperature are one-atmosphere pressure and 298 K, respectively. In the meantime, the time step and total NPT simulation time are set as 1 fs (fs) and 200 picoseconds (ps). In addition, the summation method for electrostatic and van der Waals energy is the Ewald with the accuracy of 0.001 kcal/mol and Atom-based with the cut-off distance of 15.5 Å, respectively. Further, to control the temperature and pressure during MD simulations, the Nose thermostat and Andersen barostat are adopted. After the NPT equilibrium stage, more equilibrium MD simulations with the canonical (NVT, constant atom number, model volume, and simulation temperature) are conducted on the final equilibrium configurations of rejuvenators during the NPT MD simulation step. The NVT simulation parameters of atom number, temperature, time step, simulation time, thermostat, and force field are all same as the previous NPT step.

Fig. 11 illustrates the initial and equilibrium molecular configurations of four rejuvenators before and after the MD simulations. Different kinds of molecules in each rejuvenator model are displayed with distinguishable colors to observe the molecular distribution and agglomeration levels. During the MD simulations, the molecules in a multi-component model of rejuvenator gather together owing to intermolecular force under the external pressure and temperature, resulting in the volume shrinkage of the whole molecular model. Due to the difference in the number of atoms and molecules, the cell volume and length of various rejuvenators are not compared here. However, it is interesting to discuss the molecular distribution of different molecules in multi-component molecular models of rejuvenators.

To validate the reliability of established multi-component models of various rejuvenators, the density values at 25 and 60℃ outputted from MD simulations are compared with measured values, which are summarized in Table 8. It is found that the predicted density values from MD simulations of four rejuvenators approach the experimental results at 25 and 60℃ with a divergence lower than 7%. It proves that the established multi-component model of rejuvenators, as well as the MD simulations settings of force-field, ensembles, and time steps, are reasonable. From both MD simulations and experimental results, the aromatic-oil rejuvenator exhibits the largest density value, while the density of the engine-oil rejuvenator is the lowest. Based on GC–MS analysis, more polar aromatics and fewer alkane molecules are included in the aromatic-oil rejuvenator, which leads to a stronger intermolecular force and higher density. On the other hand, the alkane molecules with low polarity and density play a dominant role in engine-oil. However, it should be noted that there is still a difference in density between the predicted and measured values. The predicted density values of bio-oil, engine-oil, and aromatic-oil are lower than the measured ones, while the naphthenic-oil shows the opposite result.

6. Performance prediction from MD simulations

The fundamentally understanding of the physical and thermodynamics properties of various rejuvenators is limited due to the difficulty of experimental measurement at the macroscale level. In this study, the MD simulations are performed on multi-component molecular models to predict the nanoscale performance of rejuvenators in terms of glass transition temperature Tg, energetic parameters, cohesive energy density and solubility parameters, volumetric parameters, dynamics behaviors (mean square distance and diffusion coefficient), structural characteristics (Radius of gyration, radial distribution function and concentration profile) and other thermodynamic properties (viscosity, activation energy, thermal expansion parameter, and isobaric heat capacity).

6.1. Glass transition temperature (Tg)

The glass transition temperature is a vital thermodynamic indicator to describe the transition point between the glassy to rubber phases, which is resulted from the mobility activation of material molecules and is strongly related to its low-temperature relaxation ability [40]. Similarly, the difference in Tg values between different kinds of rejuvenators would affect the corresponding rejuvenation efficiency in low-temperature properties of rejuvenated bitumen. However, the liquid state and low Tg characteristics of rejuvenators bring difficulty and inaccuracy to experimental measurements. Herein, the density variations of four rejuvenators are monitored to predict their glass transition temperature points [38–40]. The results are illustrated in Fig. 12, and the density values of all rejuvenators have a decreasing trend with the increase of simulation temperature. It is associated with the strong molecular mobility, large intermolecular distance, and volume expansion of the whole molecular models at high temperatures. It is worth noting that there is a turning point in the change of temperature sensitivity for all rejuvenators, which is defined as the T_g point. To calculate the T_g values of rejuvenators, the regression curves of density-temperatures before and after glass transition points are drawn in Fig. 12, and the corresponding equations are summarized in Table 9. The high values of correlation coefficient R^2 ensure the reliability of simulation outputs. Afterward, the glass transition temperatures of bio-oil, engine-oil, naphthenic-oil, and aromatic-oil rejuvenators are determined as 252.40, 237.34, 265.31, and 290.97 K, respectively. The engine-oil shows the lowest T_g value, followed by the bio-oil and naphthenic-oil, while the aromatic-oil rejuvenator presents the highest T_g indicator. It demonstrates that it is the easiest for engine-oil molecules to possess mobility at low temperatures, while the aromatic-oil molecules are still rigid and tied down until the temperature rises to 290.97 K. The difference in T_g values between various rejuvenators would lead to the difference in their rejuvenation efficiency on the low-temperature performance of aged bitumen [40].

6.2. Energetic parameters

The MD simulations are performed based on the variations of various energies of a simulation model, which results in the molecular mobility instantaneously till reaching an equilibrium state ultimately. The energetic parameters of rejuvenators depend on the molecular interactions, which are different in the multi-component molecular models of various rejuvenators. Moreover, the energetic parameters play a vital role in determining the thermodynamics properties of the simulation system. In this study, the key energetic parameters in the multi-component models of different rejuvenators are outputted and compared, including the potential energy $E_{potential}$, kinetic energy $E_{kinetic}$, non-bond energy E_{non-}

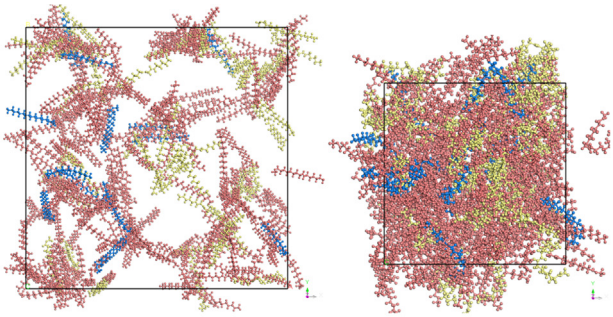

(a) Bio-oil rejuvenator

(**Blue:** Methyl Palmitate; **Yellow:** Methyl Linoleate; **Pink:** Methyl Oleate)

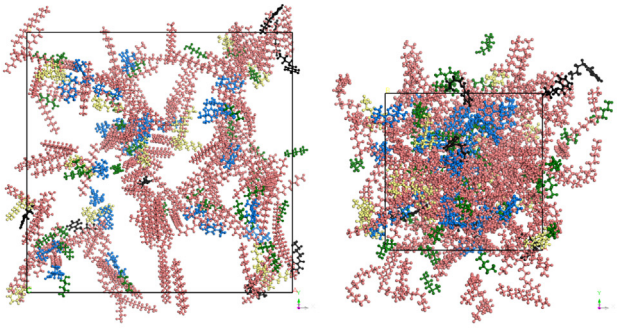

(b) Engine-oil rejuvenator

(**Pink:** Tetradecane; **Yellow:** 1-methyl-2-pentyl-Cyclohexane; **Blue:** 2,6-bis(1,1-dimenthylethyl)-phenol; **Green:** 1-Pentanol; **Black:** Butyl benzoate)

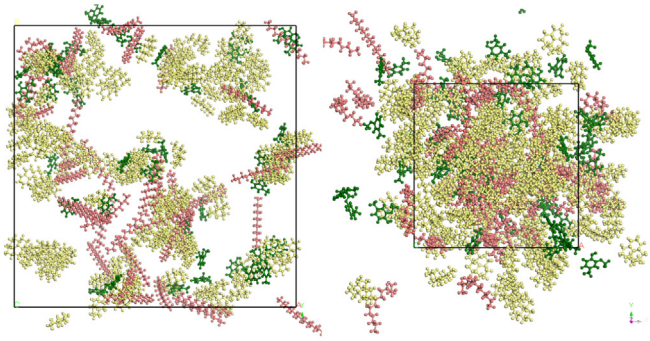

(c) Naphthenic-oil rejuvenator

(**Pink:** Tetradecane; **Yellow:** Hexadecahydro Pyrene; **Green:** 2-Methoxy-4-Methyl Phenol)

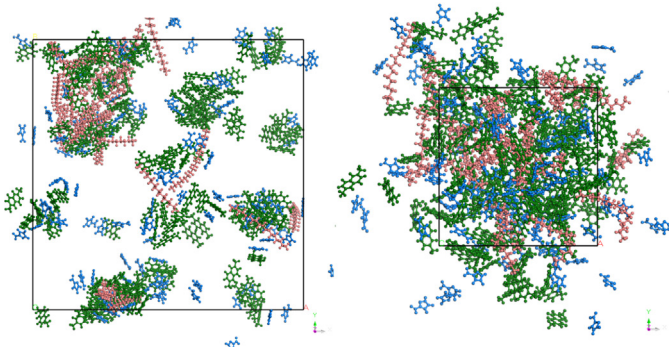

(d) Aromatic-oil rejuvenator

(**Pink:** Octadecane; **Green:** 2,7-Dimethyl naphthalene; **Blue:** Furfural)

Fig. 11. The initial and equilibrium molecular models of various rejuvenators.

Table 8
Density comparison of experimental results and MD simulation outputs.

Rejuvenators	Bio-oil	Engine-oil	Naphthenic-oil	Aromatic-oil
25℃ density ($g{\cdot}cm^{-3}$) (Exp.)	0.911	0.833	0.875	0.994
25℃ density ($g{\cdot}cm^{-3}$) (MD)	0.871	0.800	0.933	0.987
Divergence	4.39%	3.96%	6.63%	0.70%
60℃ density($g{\cdot}cm^{-3}$) (Exp.)	0.899	0.814	0.852	0.978
60℃ density ($g{\cdot}cm^{-3}$) (MD)	0.841	0.774	0.906	0.954
Divergence	6.45%	4.91%	6.34%	2.45%

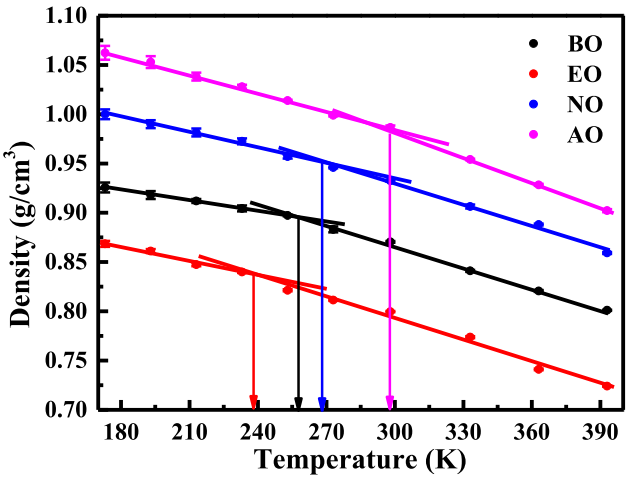

Fig. 12. The density variations of rejuvenators as a function of temperature.

$_{bond}$, total energy E_{total}, van der Waals energy $E_{van\ der\ Waals}$, electrostatic energy $E_{electrostatic}$, diagonal energy $E_{diagonal}$, and cross-terms energy E_{cross}. The relationships between these energetic parameters are displayed in **Equations 1–4**.

$$E_{total} = E_{potential} + E_{kinetic} = (E_{valence} + E_{non-bond}) + E_{kinetic}$$
$$= [(E_{diagonal} + E_{cross}) + E_{non-bond}] + E_{kinetic} \quad (1)$$

$$E_{diagonal} = E_{bond} + E_{angle} + E_{torsion} + E_{inversion} \quad (2)$$

$$E_{cross} = E_{stretch-stretch} + E_{stretch-bond-stretch} + E_{stretch-torsion-stretch} + E_{separated-stretch-stretch} + E_{torsion-stretch} + E_{bend-bend} + E_{torsion-bend-bend} + E_{bend-torsion-bend} \quad (3)$$

$$E_{non-bond} = E_{van\ der\ Waals} + E_{electrostatic} + E_{hydrogen\ bond} \quad (4)$$

For a brief introduction, the total energy is a sum of potential energy and kinetic energy, while the potential energy is composed of the diagonal energy, cross-terms energy, and non-bond energy. In addition, the diagonal energy consists of the bond energy E_{bond}, angle energy E_{angle}, torsion energy $E_{trosion}$, and inversion energy $E_{inversion}$. Meanwhile, the cross-terms energy comes from different changes of molecular configurations in terms of the stretch-stretch, stretch-bond-stretch, stretch-torsion-stretch, separated-stretch-stretch, torsion-stretch, bend-bend, torsion-bend-bend, and bend-torsion-bend. Lastly, the intermolecular interaction is mainly described with the non-bond energy $E_{non-bond}$, which contains the van der Waals energy, electrostatic energy, and potential hydrogen bond energy.

The energetic parameters of four rejuvenators at 213 K (lower temperature than Tg point), 298 K (room temperature), and 363 K (high-temperature point) are illustrated in Fig. 13. It is demonstrated that these energetic parameters at different temperatures are variable. Apart from the cross-terms energy, all energetic parameters show an increasing trend as the temperature rises. Meanwhile, the influence of temperature on the kinetic energy is slightly less than potential energy, while the non-bond energy is more dependent on temperature than the diagonal and cross-terms energies. Besides, the difference in van der Waals energy of rejuvenators as a function of temperature is much more significant than the electrostatic energy. When the temperature is the same, the positive value for the potential energy of aromatic-oil is much larger than the others, which all display negative values. The high potential energy of aromatic-oil mainly comes from the large diagonal energy. Besides, the aromatic-oil model displays the highest cross-terms energy. The reason can be explained from the viewpoint of molecular structures. In the multi-component molecular model of aromatic-oil, the main molecule is the 2,7-dimethyl naphthalene. Its double aromatic ring structure results in higher polarity and valence energy than the main molecules (methyl oleate, tetradecane, and hexadecahydro pyrene) in the multi-component molecular models of bio-oil, engine-oil, and naphthenic-oil. That's why the aromatic-oil model has the lowest kinetic energy, but the largest potential energy leads to its highest total energy value.

The engine-oil and naphthenic-oil models show similar levels of potential energy, kinetic energy, and total energy, which are all lower than that of bio-oil rejuvenators. Regarding the non-bond energy, the bio-oil model presents the lowest value, followed by the aromatic-oil and naphthenic-oil, while the engine-oil shows the highest non-bond energy. It can be found that the lowest non-bond energy of bio-oil is mainly because it has the smallest van-der Waals energy, although it shows the positive and highest electrostatic energy. Based on the current multi-component molecular models, the van der Waal energy values of engine-oil, naphthenic-oil, and aromatic-oil are similar, and the reason is complex because there are different kinds of molecules in the molecular models of various rejuvenators. As to the electrostatic energy, the naphthenic-oil, and aromatic-oil display similar values, which are much lower than engine-oil and bio-oil rejuvenators. The ranking of diagonal energy and cross-terms energy for the multi-component models of four rejuvenators is AO > BO > NO > EO and AO > EO > NO > BO, respectively.

Table 9
The correlation equations between temperature and density values of rejuvenators.

Rejuvenators	Equation (1)	R^2	Equation (2)	R^2
BO	ρ = -3.50E-4*T + 0.9860	0.9964	ρ = -6.69E-4*T + 1.0649	0.9932
EO	ρ = -5.78E-4*T + 0.9707	0.9674	ρ = -7.25E-4*T + 1.0097	0.9804
NO	ρ = -5.17E-4*T + 1.0903	0.9801	ρ = -6.89E-4*T + 1.1344	0.9897
AO	ρ = -6.35E-4*T + 1.1739	0.9943	ρ = -8.87E-4*T + 1.2505	0.9995

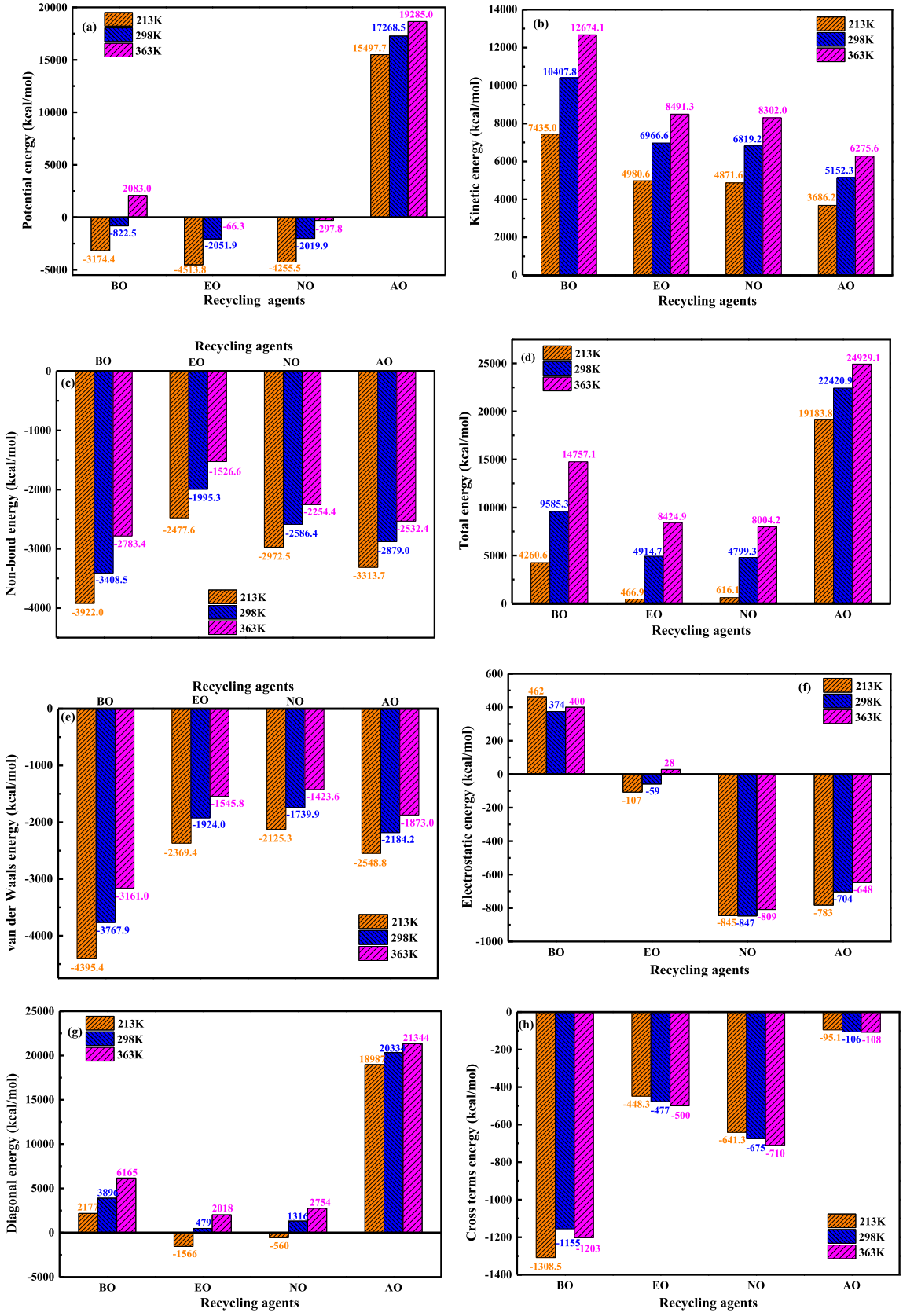

Fig. 13. The energetic parameters of different rejuvenators.

6.3. Cohesive energy density and solubility parameter

Another two important thermodynamic parameters of cohesive energy density (CED) and solubility parameter come from the energetic terms that are most popular to evaluate the intermolecular interaction and compatibility, which are calculated using **Equations (5) and (6)**. It was reported that the higher the CED value is, the more difficult for molecules to evaporate from the body model. Meanwhile, the difference in solubility parameters is an effective indicator to assess the solubility degree and compatibility between different kinds of substances.

$$CED_{total} = \frac{E_{coh}}{V} \quad (5)$$

$$\delta = (CED_{total})^{0.5} = (\delta_{vdW}^2 + \delta_{ele}^2)^{0.5} \quad (6)$$

Where E_{coh} is the total cohesive energy, J; V refers to the model volume, cm^3; δ_{vdW} and δ_{ele} represent the van der Waals-based and electrostatic-based solubility parameters.

Fig. 14 shows the CED and solubility parameter values of four rejuvenators with the total, van der Waals, and electrostatic terms at 298 K. It is found that the van der Waals-based CED and solubility parameter values for all rejuvenators are close to the total values and much larger than the electrostatic terms. It denotes that the van der Waal force is the dominant intermolecular interaction in multi-component molecular models of all rejuvenators. Regarding the total CED and solubility parameter, the magnitude order of the four rejuvenators is AO > BO > NO > EO. The aromatic-oil rejuvenator exhibits the largest CED value, indicating that the intermolecular force in the multi-component molecular model of aromatic-oil is the strongest. The reason is related to the high aromaticity and polarity characteristics of 2,7-dimethyl naphthene molecules with high dosage in the aromatic-oil model. Meanwhile, the Π-Π conjugations between condense aromatic rings in 2,7-dimethyl naphthene significantly enhance the intermolecular interactions of the aromatic-oil model. In addition, the furfural molecules with furan ring and aldehyde group also contribute to the improved intermolecular force of the whole aromatic-oil system.

In the multi-component molecular model of bio-oil rejuvenator, all kinds of molecules belong to the fatty acid esters combined with the unsaturated alkyl chain and an ester group. The polar ester group (-C = O-O-C-) in methyl palmitate, methyl linoleate, and methyl oleate molecules initiate the formation of hydrogen bonds, which are stronger than the van der Waals and electrostatic intermolecular forces but lower than Π-Π conjugations [39,49]. That's why the CED and solubility parameter values of the bio-oil molecular model are smaller than aromatic-oil but higher than that of naphthenic-oil and engine-oil. Further, it is found that the naphthene-oil multi-component model has higher CED and solubility parameter values than the engine-oil model. The multi-component molecular model of naphthenic-oil is composed of hexadecahydro pyrene (65.0%), tetradecane (19.2%) and 2-methoxy-4-methyl (15.8%), while the multi-component model of engine-oil contains the tetradecane (67.9%), 1-methyl-2-pentyl-cyclohexane (6.3%), 2,6-bis (1,1-dimethyl ethyl)-phenol (13.9%), 1-pentanol (8.1%), and butyl benzoate (3.8%). Considering the main molecular compositions, the hexadecahydro pyrene molecules in naphthenic-oil model show larger polarity and stronger intermolecular force from conjugate effects between the polycyclic cycloalkane structures than the tetradecane molecules in engine-oil [19,28]. On the other hand, the aromatic-oil model also presents the highest electrostatic-based CED and solubility parameter values, followed by the engine-oil, while the bio-oil and naphthenic-oil are at a similar level. The high concentrations of 2,7-dimethyl naphthene and furfural molecules result in the large electrostatic energy in the multi-component molecular model of aromatic oil. Meanwhile, the high electrostatic-based CED and solubility parameter values of the engine-oil model are related to the hydrocarbons in the additives group with significant polarity and aromaticity.

6.4. Volumetric parameters

It is of great significance to predict and explore the volumetric indicators of multi-component molecular models of various rejuvenators, which are strongly associated with their thermodynamics properties. In this study, the total, occupied and free volumes of different rejuvenators are measured at different temperatures. Fig. 15 visualizes these volumetric characteristics of equilibrium multi-component molecular models of bio-oil, engine-oil, naphthenic-oil and aromatic-oil rejuvenators at 298 K. Different colors represent the various kinds of molecules in multi-component models of rejuvenators. It demonstrates that the total volume refers to the volume of the whole cubic simulation unit. Meanwhile, the occupied volume shows the sum of molecular volumes in multi-component models of rejuvenators. Further, the difference between the total volume and occupied volume is defined as the free volume, which is the sum of intermolecular space in one cubic simulation unit. Due to the periodic boundary condition, the volumetric parameters from each simulation unit of multi-

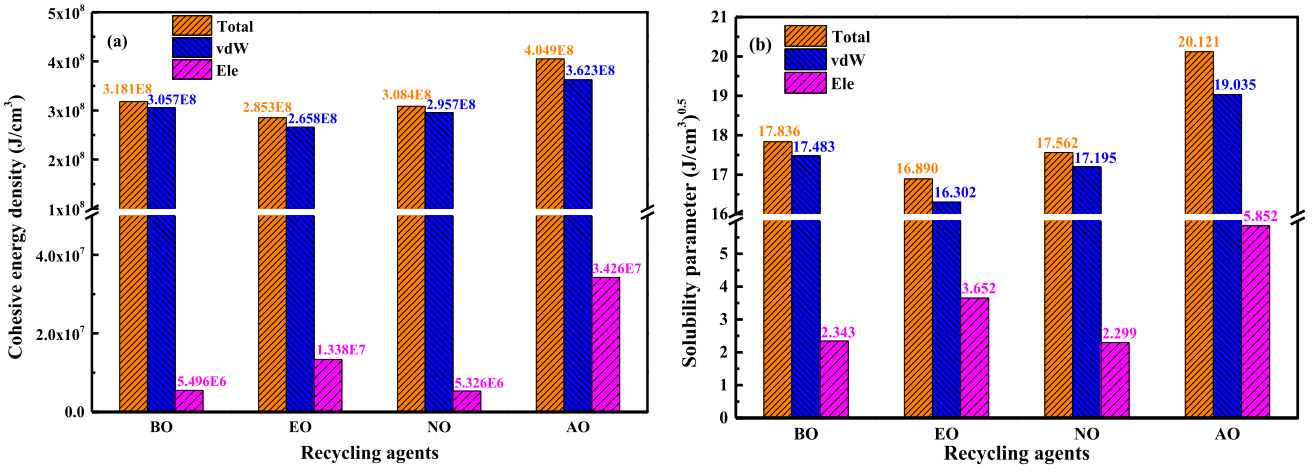

Fig. 14. The CED and solubility parameter values of different rejuvenators.

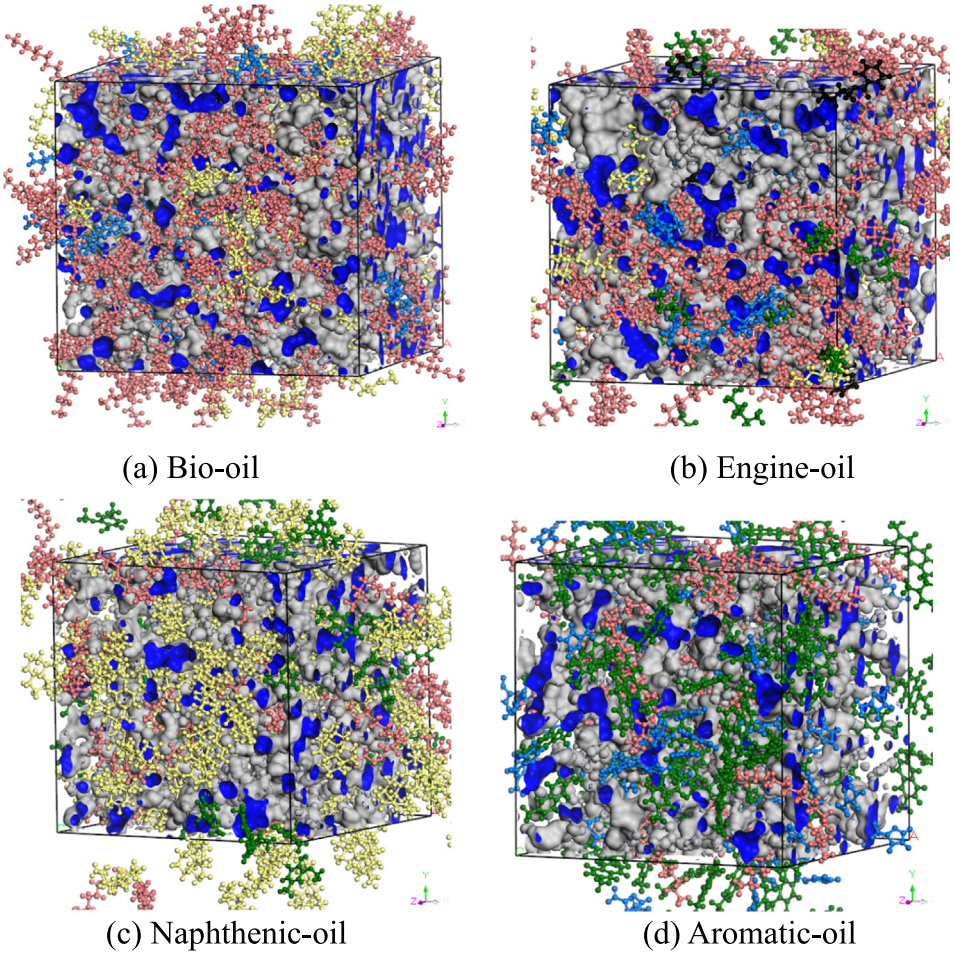

Fig. 15. The free volume calculations on equilibrium molecular models of rejuvenators.

component molecular models of rejuvenators are the same. To be more vivid, the free volume spaces in all equilibrium multi-component molecular models of rejuvenators are marked with grey-blue shapes.

The quantitative volumetric parameters for the multi-component molecular models of four rejuvenators are shown in Fig. 16a. As expected, the occupied volumes in multi-component molecular models of all rejuvenators are much larger than the free volumes. When the molecular number in each rejuvenator model is the same, the molecular volume mainly determines the occupied volume of the whole rejuvenator model. However, there is a huge difference in volumetric parameters between various rejuvenators. It is found that the bio-oil rejuvenator exhibits the largest total, occupied, and free volumes, followed by the engine-oil and naphthenic-oil, while the multi-component molecular model of aromatic-oil shows the lowest volumetric parameters. The reason can be explained from the viewpoint of molecular volume and configuration. In the multi-component model of bio-oil rejuvenator,

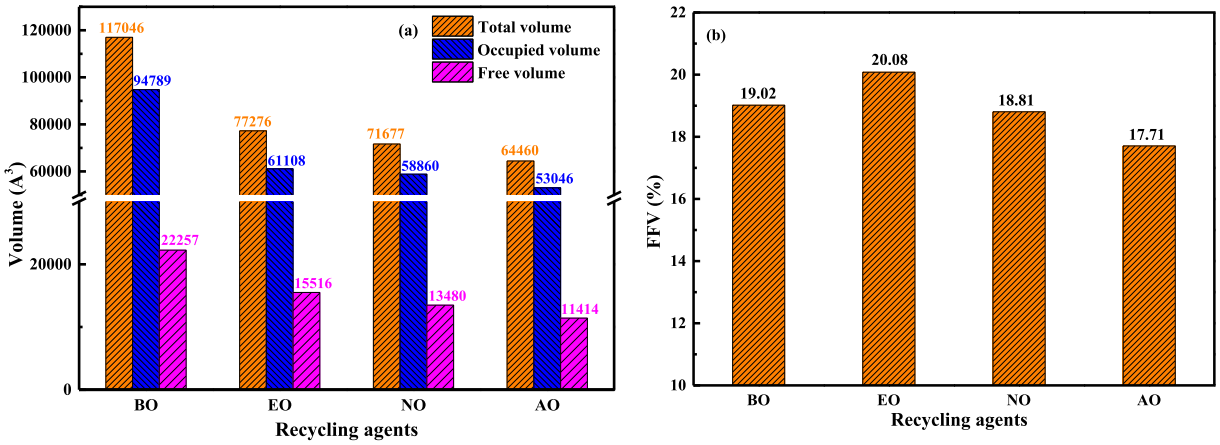

Fig. 16. The volumetric parameters and FFV of different rejuvenators at 298 K.

the fatty acid esters molecules show a large molecular size and intermolecular distance because of the long-alkane chain in their molecular structures. For the tetradecane as the main molecule in the multi-component model of engine-oil, there are 14 carbon atoms in its main molecular body, which is shorter than the alkane chain of bio-oil molecules.

Regarding the multi-component molecular models of naphthenic-oil and aromatic-oil rejuvenators, their lower volumetric parameters are not only related to the smaller molecular volume but also the stronger intermolecular forces. The polycyclic cycloalkanes structure in hexadecahydro pyrene as the main molecule of the naphthenic-oil model leads to its smaller molecular size. Moreover, the 2,7-dimethyl naphthalene and furfural molecules in the multi-component model of aromatic-oil show the smallest molecular size due to the aromatic and furan rings with a short side chain. On the other hand, compared to bio-oil and engine-oil rejuvenators, the naphthenic-oil and aromatic-oil have more polar molecules, resulting in stronger intermolecular interaction and a narrower intermolecular space.

The free volume is the main focus because it is strongly related to the relaxation and flowability performance of rejuvenators [40]. To directly compare the free volume ratio of various rejuvenators and eliminate the effect of differences in the number of molecules, a new indicator of fractional free volume (FFV) is proposed and defined as **Equation (7)**.

$$FFV = \frac{V - V_0}{V} \tag{7}$$

where FFV, V, and V_0 represent the fractional free volume, total volume, and occupied volume.

Fig. 16b shows the FFV values of four rejuvenators at 298 K, which are in the region of 17–21%. Besides, the FFV order for the multi-component molecular models of rejuvenators is EO > BO > NO > AO. The engine-oil rejuvenator exhibits the highest FFV value of 20.08%, followed by the bio-oil (19.02%) and naphthenic-oil (18.81%). Besides, the FFV value of the multi-component molecular model of aromatic-oil is the lowest at 17.71%. The polar ester groups in bio-oil molecules enhance the intermolecular interaction and reduce the free volume concentration through the formation of hydrogen bonds. Further, the high polarity and low molecular size of aromatic-oil molecules both contribute to the low fractional free volume of the multi-component molecular model of aromatic-oil rejuvenator.

On the other hand, the influence of temperature on volumetric parameters of various rejuvenators is investigated. Fig. 17 illustrates the variations of occupied and free volumes in multi-component molecular models of rejuvenators as a function of temperature. The space with red color is the occupied volume, while the blue part refers to the free volume. For all rejuvenators, with the temperature increasing, the free volume enlarges significantly. As the temperature rises from 173 K to 393 K, the free volume distribution changes from a sporadic state to island-like, which provides more free space for rejuvenator molecules to flow and relax at high external stress.

The quantitative analysis of the volumetric parameters of four rejuvenators at different temperatures is described in Fig. 18. For all rejuvenators' models, the influence of temperature on the occupied volumes is insignificant, indicating that the molecular volume is not dependent on the temperature. Meanwhile, as the temperature increases, the total and free volumes show a similar increasing trend with an apparent turning point, which is the glass transition temperature T_g. When the temperature exceeds the T_g point, the growth rates of total and free volumes strengthen due to the large molecular mobility and intermolecular space. Besides, it is revealed that the temperature effect on the whole volume of the rejuvenator model is mainly through the variation of free volume. The temper-

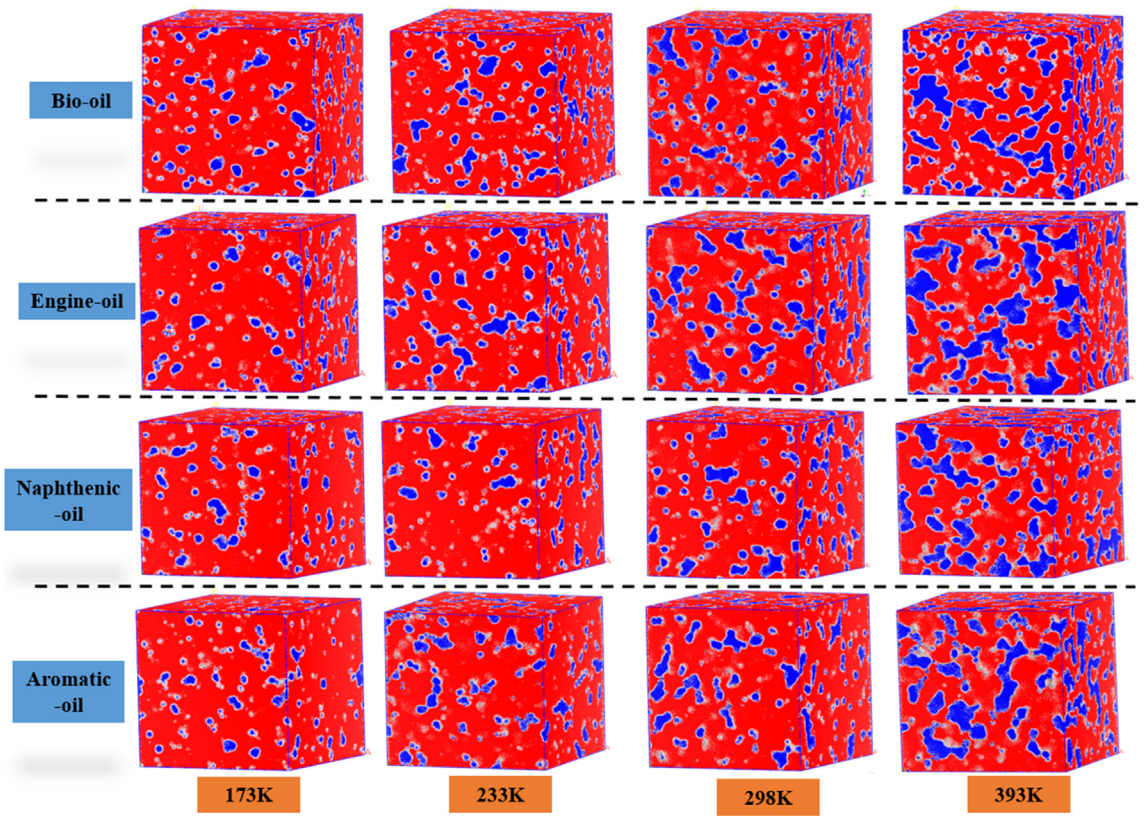

Fig. 17. Influence of temperature on free volume distributions of four rejuvenators (Red color: Occupied volume; Blue color: Free volume).

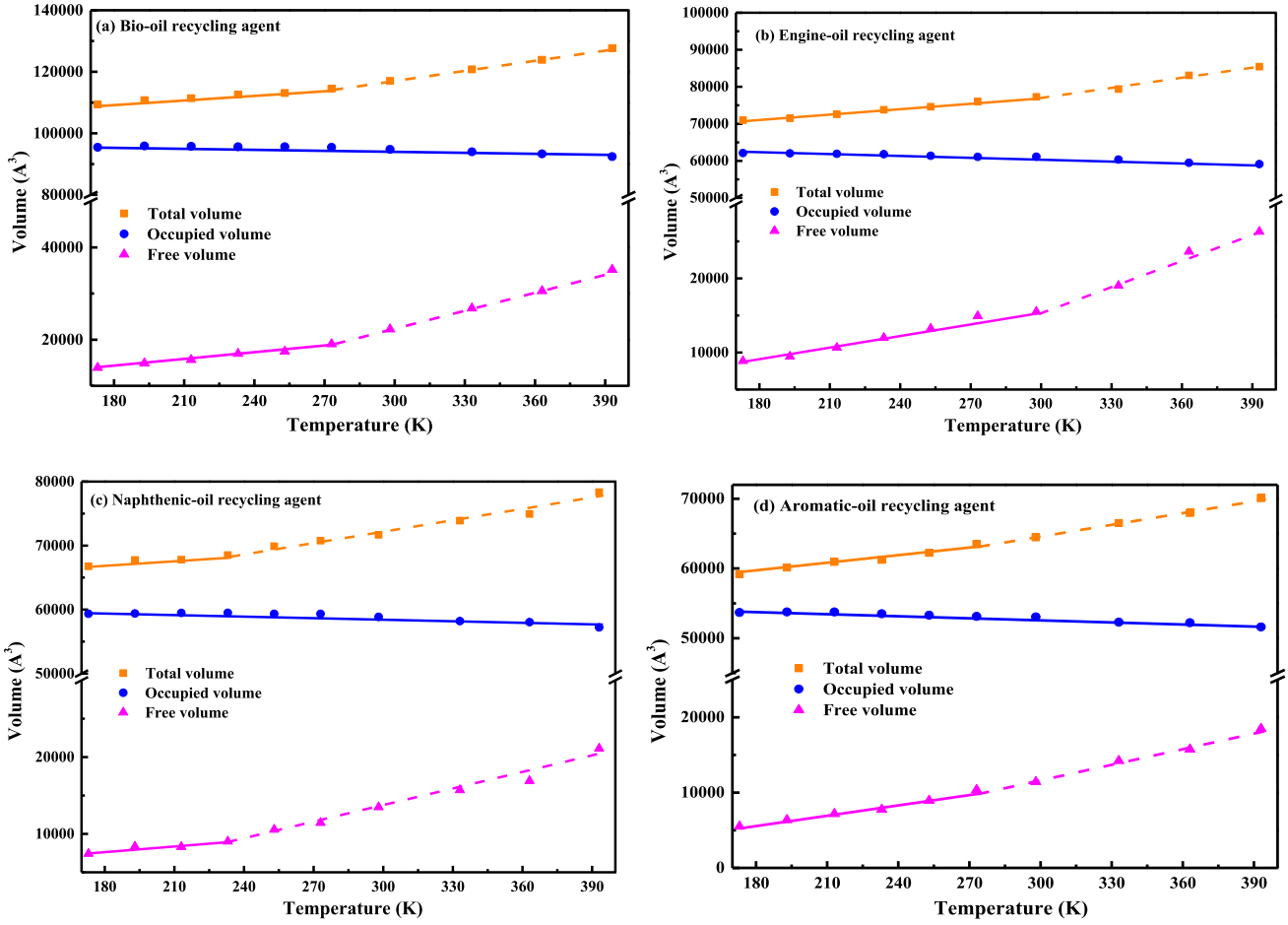

Fig. 18. Influence of temperature on volumetric parameters of different rejuvenators.

ature dependence of volumetric parameters for four rejuvenators will be discussed in the following section through a new parameter of the thermal expansion coefficient.

Fig. 19a draws the variation of FFV values of four rejuvenators as a function of simulation temperature, which displays an increasing trend with the increase of temperature. When the temperature rises from 173 K to 393 K, the FFV values of bio-oil, engine-oil, naphthenic-oil and aromatic-oil rejuvenators increase from 12.7%, 12.5%, 11.1%, and 9.3% to 27.6%, 30.8%, 27.0%, and 26.4%, respectively. In addition, the FFV parameters of the multi-component molecular models of four rejuvenators follow the decreasing order of EO > BO > NO > AO. Due to the existence of free volume, the surface area in the multi-component molecular model is apparent, which would affect the diffusion rate of other substances (like oxygen and moisture) in rejuvenators. The surface area values of four rejuvenators at different temperatures are displayed in Fig. 19b. As expected, the surface area of the rejuvenator remarkably increases with the temperature rising. It indicates that high temperature would increase the interaction area of the rejuvenator with oxygen and moisture molecules, thus intensifying their diffusion and interaction with the molecules of rejuvenators. Moreover, the magnitude order of molecular surface in multi-component models of four rejuvenators is shown as BO > EO > NO > AO. It implies that the bio-oil rejuvenator provides the highest interaction area with oxygen or moisture molecules, while it is the most difficult for oxygen and moisture molecules to diffuse in an aromatic-oil rejuvenator. Therefore, it is speculated that the resistance to oxidative aging and moisture influence of aromatic-oil rejuvenator is the best, while it is the easiest for the bio-oil rejuvenator to suffer from oxidation aging and moisture penetration. However, the hypothesis should be further verified based on experimental results.

6.5. Dynamic behaviors

The dynamic molecular mobility of the multi-components molecular models of four rejuvenators is assessed by the parameters of mean square displacement (MSD) and diffusion coefficient (D), which are obtained following **Equations (8) and (9)**.

$$MSD(t) = < \Delta r_i(t)^2 > = < [r_i(t) - r_i(0)]^2 > \quad (8)$$

$$D = \frac{1}{6N} \lim_{t\to\infty} \frac{d}{dt} \sum MSD(t) = \frac{a}{6} \quad (9)$$

where MSD(t) represents the mean square displacement of the rejuvenator model at simulation time t (ps), Å^2; r_i (0) and r_i (t) refers to the initial and current coordinate, Å; D is the diffusion coefficient, m^2/s; N shows the total number of molecules in the multi-component model of rejuvenator; a is the slope value in correlation equation between MSD and time.

The MSD values of different rejuvenators as a function of simulation time at 298 K are monitored and shown in Fig. 20a. It is found that the MSD values increase linearly as the time prolongs, and the correlation equations between MSD and t of four rejuvenators are also listed. When the simulation time keeps constant, the magnitude order of MSD values for the multi-component models of four rejuvenators is as follows: AO > EO > NO > BO. Meanwhile, the diffusion coefficient values of rejuvenators are calculated and pre-

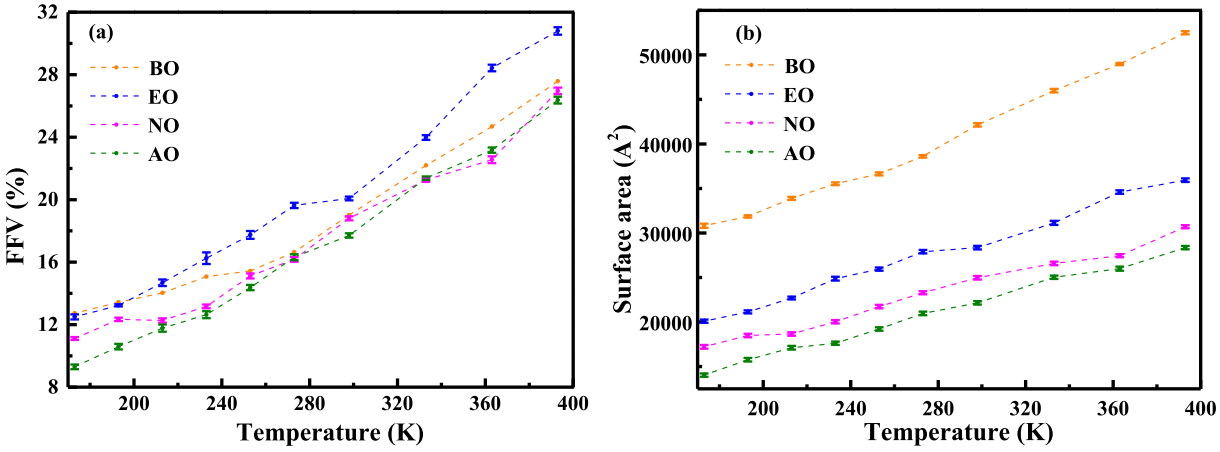

Fig. 19. Influence of temperature on FFV and surface area of different rejuvenators.

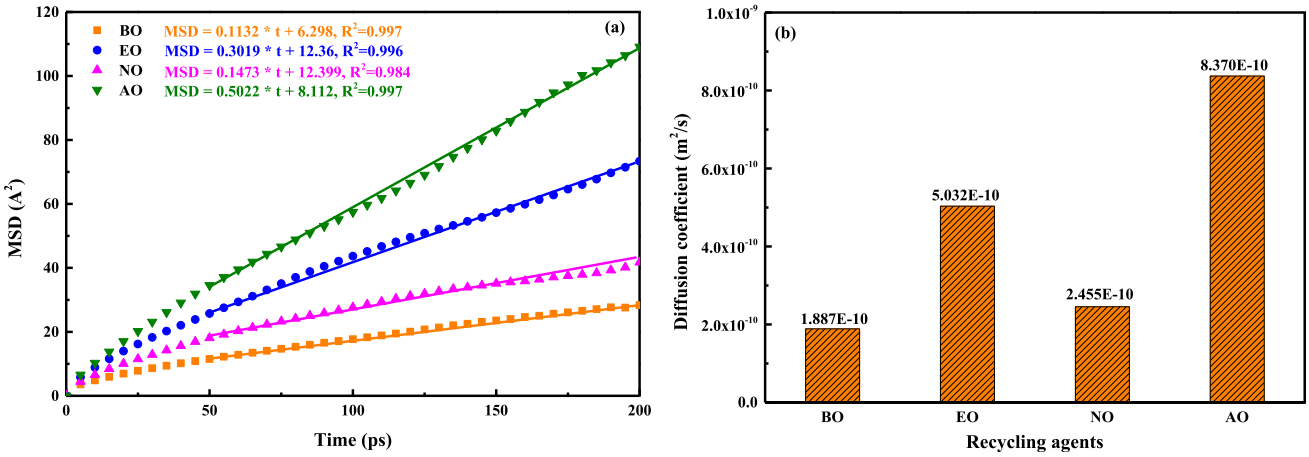

Fig. 20. The MSD and diffusion coefficient of rejuvenators at 298 K.

sented in Fig. 20 **b**. The aromatic-oil rejuvenator exhibits the highest diffusion coefficient of 8.37E-10 m^2/s, followed by engine-oil (5.032E-10 m^2/s) and naphthenic-oil (2.455E-10 m^2/s), while the diffusion coefficient of the bio-oil rejuvenator is the smallest of 1.887E-10 m^2/s. The result is out of an expectation that the aromatic-oil rejuvenator should exhibit the lowest dynamic performance due to its large molecular weight and intermolecular forces. The reason for the unexpected phenomenon can be explained that from the GC–MS test, the 2,7-dimethyl naphthene molecule is detected as the main molecule of aromatic-oil, but it is difficult to monitor the aromatic molecules with>2 fused aromatic rings because of their heavy molecular weight. It leads to the negligence of these large aromatic molecules in the multi-component molecular model of aromatic-oil rejuvenator. Meanwhile, the incorporation of furfural molecules with a high dosage of 57.5% plays a crucial role in enhancing the molecular mobility of the 2,7-dimethyl naphthalene. It is concluded that the GC–MS method is not able to measure all chemical components in aromatic-oil rejuvenators, and the large aromatic molecules should be considered in the molecular model of aromatic-oil.

For the other three rejuvenators, it is expected that the diffusion coefficient of naphthenic-oil is lower than engine-oil. It is because more alkane molecules (tetradecane) exist in engine-oil than naphthenic-oil. Moreover, the diffusion coefficient of the hexadecahydro pyrene as the main molecule of naphthenic-oil is much lower than the tetradecane alkane molecule. Regarding the bio-oil rejuvenator, the long carbon chain in fatty acid esters hinders the molecular diffusive ability. Besides, the formation of hydrogen bonds increases the intermolecular force and reduces the mobility of molecules in bio-oil. It should be mentioned that the MSD values of rejuvenators are the sum of the MSD of each molecule in their multi-component molecular models. It is still difficult to explain the underlying reason for the difference in MSD and diffusion coefficient values between the multi-component molecular models of various rejuvenators. Thus, the MSD and diffusion coefficient values of each molecule in different rejuvenators are measured, and the results are shown in **Figures S4 and S5**.

Temperature plays a key role in affecting molecular mobility and diffusive behaviors. The temperature dependence of multi-component molecular models of four rejuvenators is evaluated through the variation of MSD and diffusion coefficient parameters. Fig. 21 displays the MSD values of four rejuvenators at different temperatures. As the temperature grows, the MSD parameter increases distinctly when the simulation temperature keeps constant. It implies that a higher temperature accelerates the stronger mobility of molecules in all multi-component models of four rejuvenators. In addition, the temperature effect on the MSD values of rejuvenator molecules becomes more distinct when the temperature exceeds 333 K. Based on the slope values in MSD-time regressive equations, it is demonstrated that the temperature-dependence of MSD parameters for four rejuvenators. The diffusion coefficient values of multi-component molecules of rejuvenators at

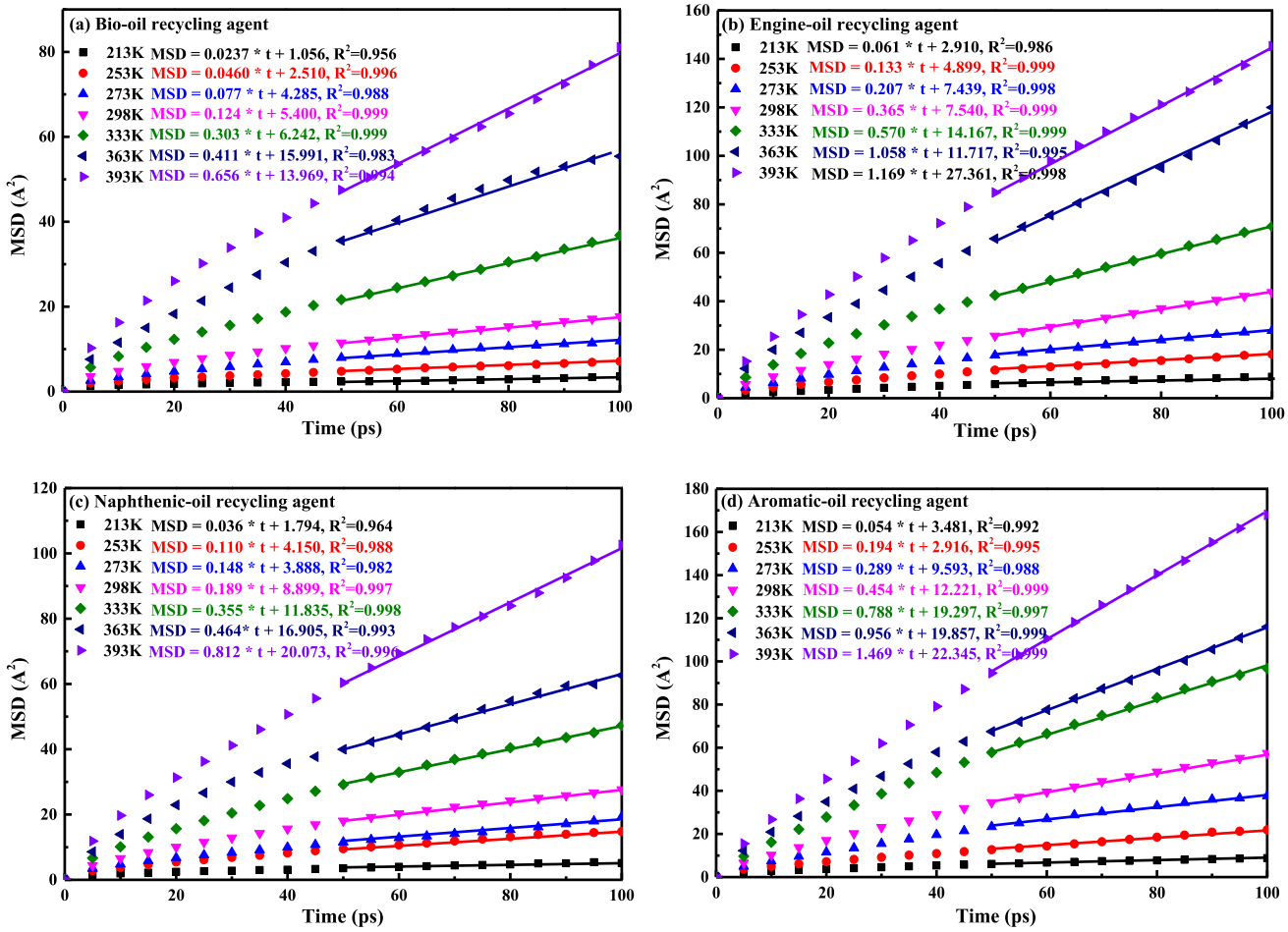

Fig. 21. Influence of temperature on MSD values of rejuvenators.

different temperatures are calculated and listed in Table 10. The growing temperature increases the diffusion coefficient of four rejuvenators. When the temperature rises from 213 to 393 K, the diffusion coefficient of bio-oil, engine-oil, naphthenic-oil and aromatic-oil increase from 3.95E to 11, 1.017E-10, 6.0E-11, and 9.0E-11 to 1.09E-9, 1.95E-9, 1.35E-9, and 2.49E-9 m^2/s. Meanwhile, the difference in diffusion coefficient values between the four rejuvenators becomes less significant at high temperatures. Further, the diffusion coefficient ranking at all temperatures for four rejuvenators is AO > EO > NO > BO.

To further assess the temperature sensitivity of the diffusion coefficient parameter for four rejuvenators, the Arrhenius equation (**Equation (10)**) is adapted to fit the correlation curves between the diffusion coefficient (LnD) and the reciprocal value of temperature (1/T).

$$D = A\exp\left(\frac{-E_a}{RT}\right) \tag{10}$$

where D and T are the diffusion coefficient (m^2/s) and temperature (K); Ea refers to the activation energy (J/m^2); A and R represent the pre-exponential factor and universal gas constant (8.314 $J/mol{\cdot}K^{-1}$).

The correlation curves and equations are all plotted in Fig. 22. The high R^2 values denote that the Arrhenius equation can well fit the LnD-(1/T) curves of all rejuvenators. The temperature sensitivity of different rejuvenators is reflected by the absolute slope value, which follows the ranking as BO > AO > EO > NO. Besides, the Ea values of bio-oil, engine-oil, naphthenic-oil, and aromatic-oil are 13336.7, 12058.0, 11400.7, and 12455.7 J/m^2, respectively. It suggests that the multi-component molecular model of naphthenic-oil exhibits the lowest temperature sensitivity, followed by the engine-oil and aromatic-oil, while the bio-oil is the most sensitive to temperature. This conclusion will be further verified by viscous property in the following section 6.7.

6.6. Structural indicators

Apart from the molecular compositions, the difference in the micro-and-macroscales properties between various rejuvenators is strongly connected with the molecular structures and arrangements. In this study, the structural indicators, radial of gyration (R_g), radial distribution function (RDF), and relative concentration of different molecules in multi-component molecular models of four rejuvenators, are calculated and analyzed. The R_g and g(r) are obtained through **Equations (11) and (12)**.

$$R_g = \left(\frac{\sum r_i^2 m}{\sum m}\right)^{\frac{1}{2}} \tag{11}$$

$$g(r) = \frac{dN}{4\pi r^2 \rho dr} \tag{12}$$

where m is the mass of the molecule branch, $g{\cdot}mol^{-1}$; r_i represents the distance between the mass center of a molecule to the branch, Å; N refers to the molecule number in the whole multi-

Table 10
The diffusion coefficient (D, m^2/s) of rejuvenators at various temperatures.

Temperature (K)	BO	EO	NO	AO
213	3.950E-11	1.017E-10	6.000E-11	9.000E-11
253	7.670E-11	2.217E-10	1.833E-10	3.233E-10
273	1.283E-10	3.450E-10	2.467E-10	4.817E-10
298	2.067E-10	6.083E-10	3.150E-10	7.567E-10
333	5.050E-10	9.500E-10	5.917E-10	1.313E-9
363	6.850E-10	1.763E-9	7.733E-10	1.593E-9
393	1.090E-9	1.948E-9	1.353E-9	2.448E-9

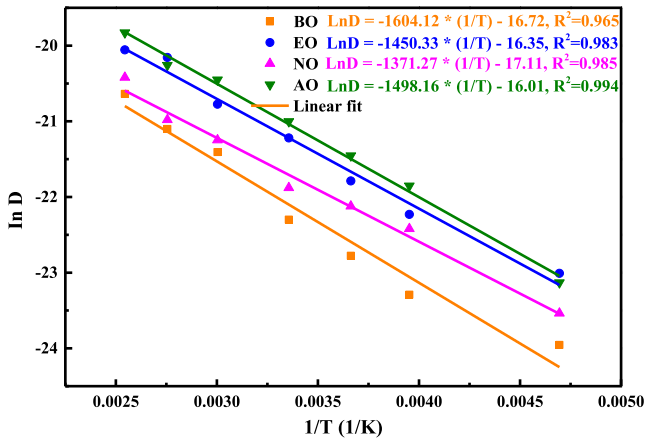

Fig. 22. The correlation between temperature and diffusion coefficient of rejuvenators.

component molecular model of rejuvenator; ρ and r are the density ($g \cdot cm^3$) and distance from the specified molecule (Å), respectively.

6.6.1. Radius of gyration R_g

Fig.23a-d illustrates the probability density distribution of the R_g of the multi-component molecular model of bio-oil, engine-oil, naphthenic-oil, and aromatic-oil rejuvenator, respectively. The total and each molecule terms are all displayed to detect the dominant molecules determining the R_g value of the whole rejuvenator system. In the multi-component molecular model of bio-oil, the probability density of the whole system, methyl oleate, methyl palmitate, and methyl linoleate shows a peak value at the R_g point of 6.3, 6.3, 6.0, and 6.2 Å, respectively. It is associated with the shorter carbon chain in methyl palmitate than the methyl oleate and methyl linoleate, which show a similar R_g distribution. In the engine-oil rejuvenator, the probability density has four peaks at the R_g of 2.2, 2.8, 3.1, and 4.6 Å, which come from different molecules. In detail, the 1-pentanol, 2,6-bis (1,1-dimethyl ethyl)-phenol, and 1-methyl-2-pentyl-cyclohexane present the maximum P-value at the R_g of 2.2, 2.8, and 3.1 Å, respectively. Moreover, the butyl benzoate molecule has two P-value peaks at 3.0 and 3.25 Å. Further, the tetradecane molecule, as the main component of engine-oil, shows a broad P-value distribution and the peak value occurs approximately at the R_g of 4.4 Å.

Regarding the probability density of naphthenic-oil, there are three peaks observed at the R_g point of 2.25, 2.6, and 4.7 Å, which represent the 2-methoxy-4-methyl phenol, hexadecahydro pyrene, and tetradecane molecule, respectively. Similarly, three peaks are detected in the R_g distribution curve of aromatic-oil, which is located at the R_g of 1.8, 2.6, and 6.0 Å. With the R_g value increasing, the P-value peak comes from the furfural, 2,7-dimethyl naphthalene, and octadecane molecule, respectively. It is depicted that the R_g values of main molecules of aromatic-oil are much lower than molecules in the other three rejuvenators, which explains why the aromatic-oil model exhibits the highest diffusive ability. However, it should be mentioned that the heavy-weight aromatic oils are not detected by the GC–MS method and are not considered in the multi-component molecular model of aromatic-oil. A more accurate method should be developed to monitor the molecular structures of heavy-weight aromatic molecules, then a more realistic multi-component molecular model of aromatic-oil can be established. In addition, compared to the molecules in engine-oil and naphthenic-oil, the bio-oil molecules show higher R_g values, which hinders molecular mobility and reduces the diffusive rate. Meanwhile, the R_g parameters of all additive molecules in engine-oil are lower than that of tetradecane (main component), indicating that the incorporation of these additive molecules promotes the enhancement in molecular mobility of engine-oil molecules. In naphthenic-oil, the R_g value of 2-methoxy-4-methyl phenol is smaller than the main molecules of hexadecahydro pyrene and tetradecane.

6.6.2. Radial distribution function RDF

The molecular arrangement in the multi-component molecular models of four rejuvenators is evaluated by the radial distribution function g(r), which represents the probability of a specific molecule appearing at a distance from the reference point. The RDF curves between different molecules in four rejuvenators are drawn in Fig. 24, including the total, self-molecular and intermolecular g (r) distribution. It is found that the molecular self-agglomeration is more significant than the intermolecular ones according to the high g(r) values of self-molecular interactions. Moreover, the g(r) values between different molecules in four rejuvenators all approach 1.0, indicating that the overall intermolecular distribution is homogeneous in the long-distance range. Meanwhile, the self-molecular agglomeration phenomenon is observed only when the intermolecular distance is lower than 5 Å. It further indicates that the molecules in the multi-component molecular model of rejuvenators are in short-distance order and long-range disorder. In the multi-component model of bio-oil, the g(r) peaks of the total, methyl oleate, methyl palmitate, and methyl linoleate pairs occur at the same positions, but the peak values are different. The methyl palmitate pair shows the highest g(r) peak values, followed by the methyl linoleate and methyl oleate pairs. It denotes that the possibility for self-molecular agglomeration of methyl palmitate pair in bio-oil is the largest. In the engine-oil model, the butyl benzoate pair shows the highest peak values, followed by the cyclohexane, pentanol, phenol, and tetradecane pairs. Meanwhile, the phenol and pentanol pairs show an additional peak at 0.9 Å, which is associated with their small molecular size. Regarding the intermolecular RDF in engine-oil, the butyl benzoate-pentanol pair has the highest g(r) peak value, followed by the phenol-pentanol pair, while the cyclohexane-pentanol presents the lowest peak value. It suggests that the possibility of intermolecular agglomerations between pentanol with benzoate and phenol are higher than others, which may be related to the oxygen-containing polar functional groups in their molecular structures.

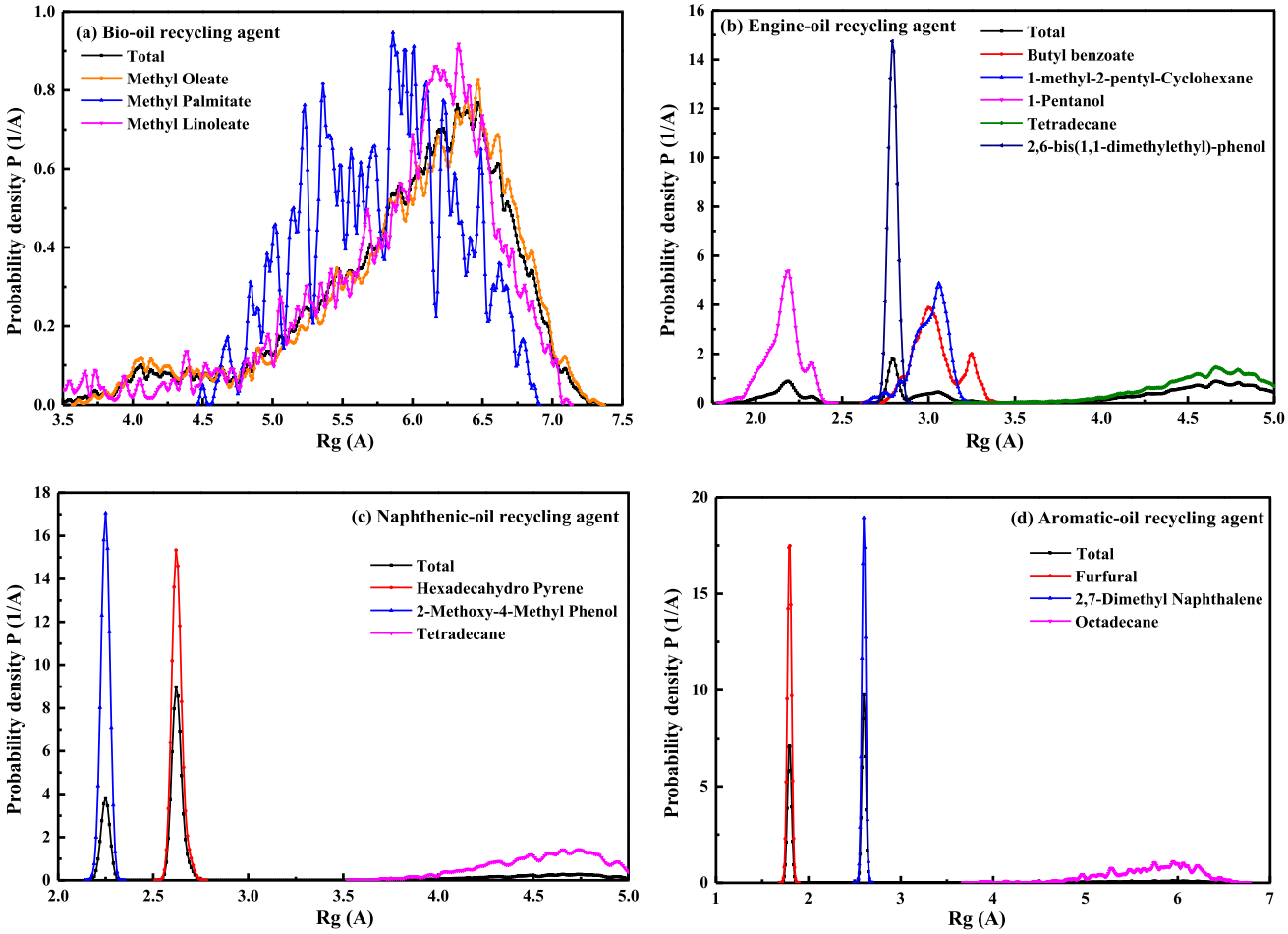

Fig. 23. The R_g distribution of different molecules in rejuvenators.

The RDF curves of the naphthenic-oil model reveal that the phenol pair shows the strongest self-molecular agglomeration potential, followed by the tetradecane and pyrene pairs. Besides, the g (r) peak value of the tetradecane-phenol pair is larger than that of tetradecane-pyrene and phenol-pyrene molecular pairs. In addition, the octadecane pair in aromatic-oil shows the highest g(r) peak values, followed by the furfural and naphthalene pairs. An additional peak at 1.2 Å for the furfural pair is observed, indicating that the intermolecular distance between furfural molecules is smaller than others in the multi-component molecular model of aromatic-oil rejuvenator. Further, the g(r) peak value of furfural-naphthalene is higher than the naphthalene-octadecane pair, while the furfural-octadecane shows the lowest peak value. It indicates that the intermolecular agglomeration degree between the furfural and naphthalene molecules is the largest, while the furfural and octadecane molecules disperse each other more homogeneously. The reason may be that the high polarity and aromatic structure enlarge the intermolecular interaction between the furfural and naphthalene molecules. In the meanwhile, the small molecular size provides more mobility to furfural molecules, which promotes the homogenous dispersion of furfural molecules in the multi-component molecular model of aromatic-oil rejuvenator.

6.6.3. Relative concentration distribution

The concentration profile was obtained by calculating the atomic density distribution of the 3D periodic structure to the coordinate axis, which is defined as the ratio of the number of atoms in the unit volume perpendicular to the axis direction to the number of atoms contained in the unit volume of the amorphous cell. Fig. 25 shows the concentration distributions in the multi-component molecular models of four rejuvenators at three directions of (100), (010), and (001). The relative concentration of 1.0 represents that the molecular distribution in the rejuvenator model is homogeneous. However, the concentration profile indicates that there is an obvious fluctuation around the value of 1.0. It means that the multi-component molecular models of four rejuvenators are inhomogeneous at the atomic level. Meanwhile, the molecular distributions in rejuvenator models are variable in different directions. Based on the lowest fluctuation amplitude, the multi-component molecular model of engine-oil is the most homogenous. Moreover, the bio-oil and naphthenic-oil show similar maximum and minimum fluctuation amplitude values. The fluctuation amplitude of the relative concentration for the multi-component molecular model of aromatic-oil rejuvenator is the highest, which is in the (010) direction. Thus, the molecular distribution in the aromatic-oil model is the most uneven.

6.7. Viscosity, thermal expansion coefficient, and isobaric heat capacity

The viscosity indicator is of great importance to evaluate the rejuvenation efficiency of different rejuvenators [24–26]. In this study, the viscosity values of four rejuvenators are predicted using the Einstein-Stokes equation as follows:

$$\eta = \frac{kT}{6\pi rD} \tag{13}$$

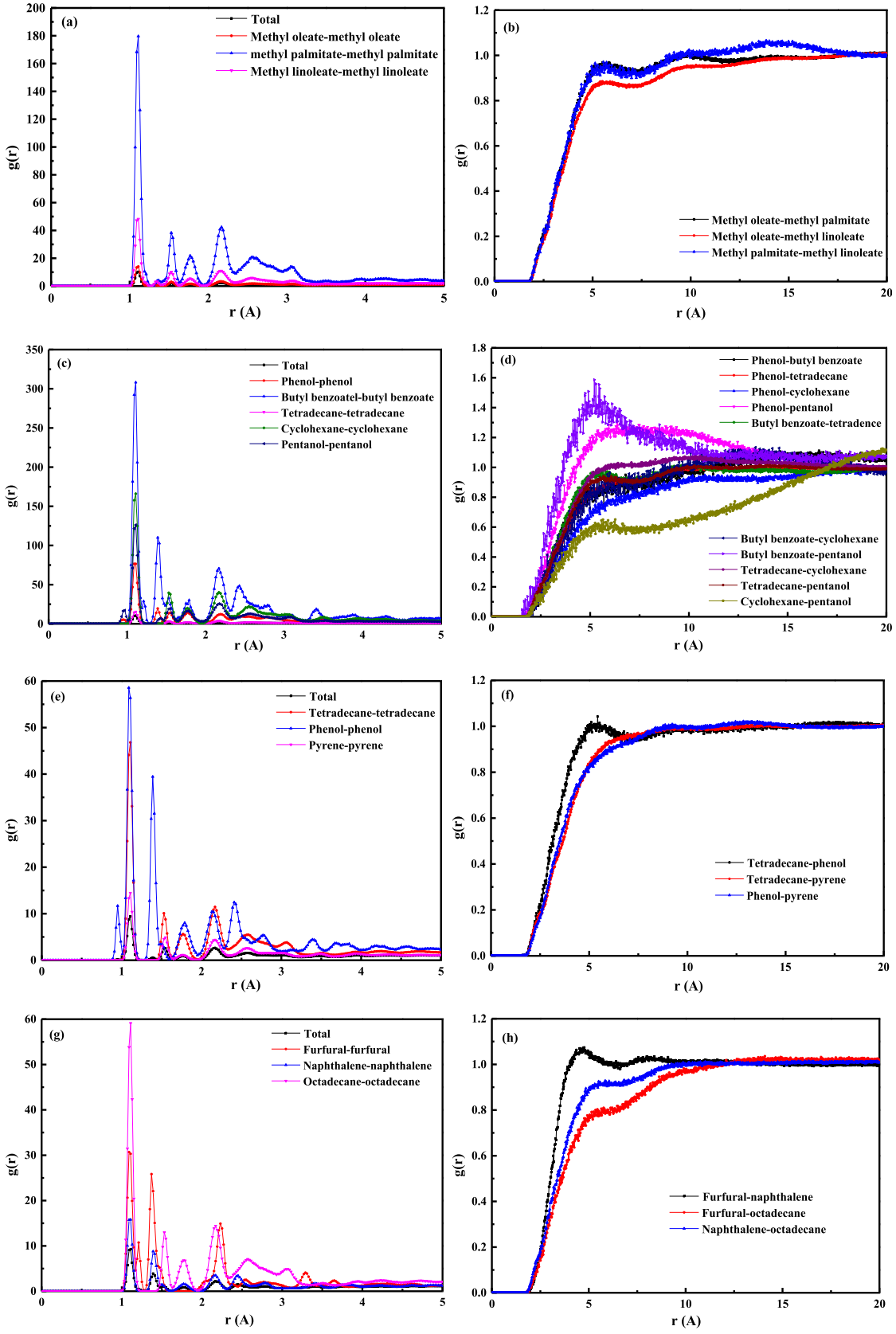

Fig. 24. The RDF distribution of different molecules in rejuvenators (a)(b) Bio-oil; (c)(d) Engine-oil; (e)(f) Naphthenic-oil; (g)(h) Aromatic-oil.

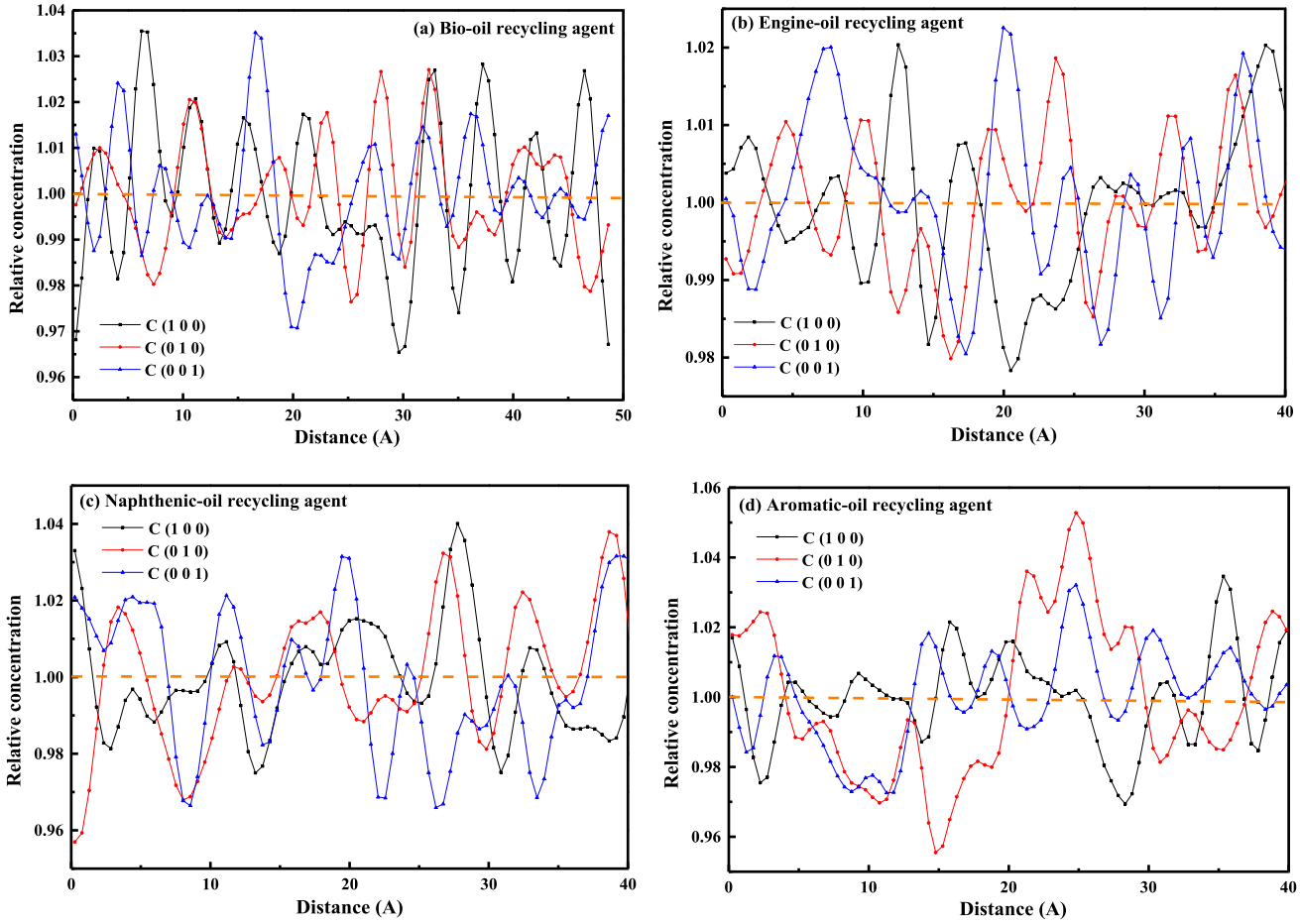

Fig. 25. The concentration distribution of different components in rejuvenators.

where η and D represent the viscosity (Pa·s) and diffusion coefficient (m^2/s); T is the temperature, K; r and k refer to the radius of gyration (m), and Boltzmann constant (1.38065E-23 J/K). The predicted viscosity values of four rejuvenators at different temperatures are measured, and the correlation curves between the Ln (η) and 1/T are plotted in Fig. 26a. As the increase of temperature, the viscosity values of all rejuvenators reduce. When the temperature is the same, the predicted viscosity of naphthenic-oil is the largest, while there is no significant difference in the predicted viscosity of the other three rejuvenators. To further validate the reliability of predicted viscosity values, the rotational viscosity of four rejuvenators is tested at different temperatures, which is shown in Fig. 26b. From the experimental results, the aromatic-oil exhibits the highest viscosity, followed by the naphthenic-oil, while the engine-oil and bio-oil show similar viscosity values. It relies on that the viscosity ranking of four rejuvenators from simulation agrees well with that from the experiment except for the aromatic-oil. The underlying reason was explained in the diffusion

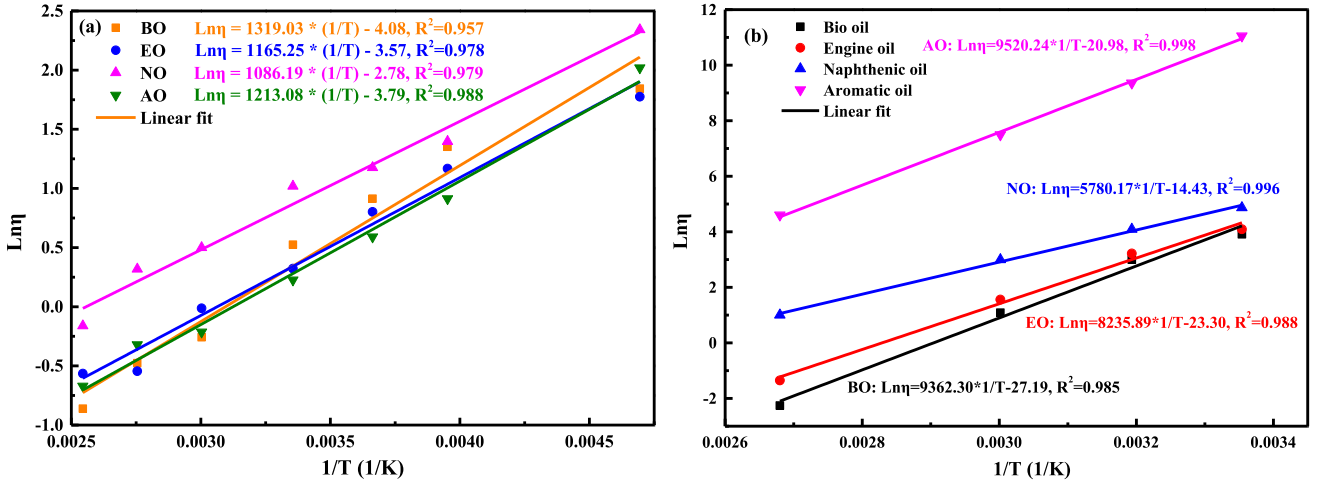

Fig. 26. Viscosity prediction and comparison of different rejuvenators (a) Predicted values; (b) Experimental results.

section that the heavy-weight aromatic molecules in aromatic-oil rejuvenator are not detected by the GC–MS method, and the negligence of these large molecules in a multi-component molecular model of aromatic-oil leads to the inaccurate simulation outputs in aspects of the strong molecular mobility and low predicted viscosity.

The temperature dependence of predicted and measured viscosity values of four rejuvenators is described by the Arrhenius formula as follows:

$$\mathrm{Ln}\eta = \frac{E_{vis}}{R}\cdot\frac{1}{T} + \mathrm{LnA} \tag{14}$$

where η and T are the viscosity (Pa·s) and temperature (K); E_{vis} refers to the viscous-flow activation energy, J/mol; A and R show the pre-exponential factor and universal gas constant (8.314 J/mol·-K-1). The calculated E_{vis} and A values of four rejuvenators from MD simulations (E_{MD} and A_{MD}) and experimental tests (E_t and A_t) are listed in Table 11. It is found that the simulation outputs present lower E_{vis} and higher A values than the experimental results. It is interesting to note that the E_{vis} and A parameters ranking for four rejuvenators from predicted viscosity agrees well with that from measured values. The naphthenic-oil rejuvenator presents the lowest E_{vis} and highest A values, followed by the engine-oil. The bio-oil and aromatic-oil show similar E_{vis} values both from MD simulations and experimental results.

Further, the thermal expansion coefficient and isobaric heat capacity of the multi-component molecular models of four rejuvenators are predicted using **Equations 15–17**.

$$\beta = \frac{1}{V}\left(\frac{\partial V}{\partial T}\right)_P \tag{15}$$

$$\alpha = \frac{1}{L}\left(\frac{\partial L}{\partial T}\right)_P \tag{16}$$

$$C_P = \left(\frac{\partial H}{\partial T}\right)_P \tag{17}$$

where V and L are the volume (Å^3) and length (Å) of the multi-component molecular model; T and P represent the variable temperature (℃) and constant pressure (10^{-4} GPa); and H refers to the total enthalpy of the rejuvenator model, kcal/mol.

Table 11
The E_{vis} and A values of four rejuvenators from MD simulations and tests.

Rejuvenators	BO	EO	NO	AO
E_{MD} (J/mol)	10966.4	9687.9	9030.6	10085.5
A_{MD}	1.69E-2	2.82E-2	6.20E-2	2.26E-2
E_t (J/mol)	77838.2	68473.2	48056.3	79151.3
A_t	1.55E-12	7.60E-11	5.41E-7	7.74E-10

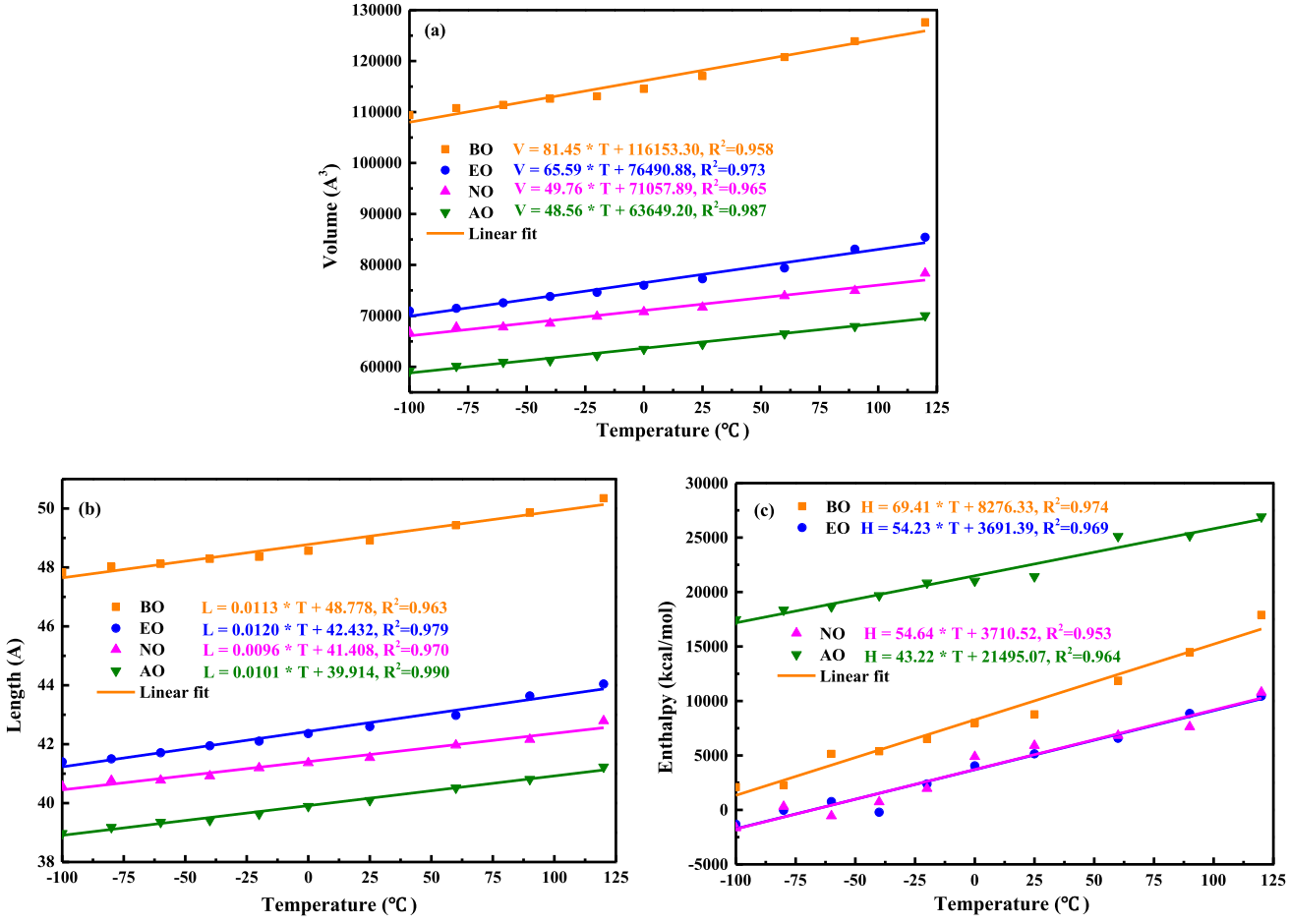

Fig. 27. The variations of volume (a), length (b), and enthalpy (c) of rejuvenators.

Table 12
Thermal expansion coefficient and isobaric heat capacity of different rejuvenators.

Rejuvenators	BO	EO	NO	AO
β (1/℃)	6.959E-4	8.488E-4	6.942E-4	7.533E-4
α (1/℃)	2.310E-4	2.818E-4	2.311E-4	2.519E-4
C_p (kcal/(mol·℃))	69.41	54.23	54.64	43.22

Fig. 27 illustrates the variations of cell volume, length, and enthalpy versus the simulation temperatures for four rejuvenators. The increase in temperature promotes the enhancement of molecular mobility and volume expansion of the whole rejuvenator system. The cell volume, cell length, and enthalpy all display positive correlations with temperature, and the corresponding correlation equations are also shown in Fig. 27. Afterward, the thermal expansion coefficient (β and α) and isobaric heat capacity (C_p) values of the four rejuvenators are derived and summarized in Table 12. The multi-component model of engine-oil exhibits the highest thermal expansion coefficient, followed by the aromatic-oil, while the bio-oil and naphthenic-oil show similar thermal expansion coefficient values. Regarding the C_p parameter, the ranking for the multi-component molecular models of four rejuvenators is BO > NO > EO > AO.

7. Conclusions and recommendations

This study aims to in-depth analyze the chemical components of four widely-used rejuvenators (bio-oil, engine-oil, naphthenic-oil, and aromatic-oil) with the Gas chromatography-mass spectrometry (GC–MS) method, and propose their multi-component molecular models for the first time. Further, the MD simulations are carried out on these multi-component models of various rejuvenators to anticipate and compare their atomic-level properties. The main findings are drawn as follows:

(1) The GC–MS results reveal that the chemical components of petroleum-based rejuvenators are more complex than the bio-oil. The alkane, naphthenic, and aromatic molecules are the main chemical component of EO, NO, and AO rejuvenators, which differ in the carbon-chain length, the number of naphthenic rings, and aromatic rings.

(2) Based on the chemical components from the GC–MS test, the main molecules in each rejuvenator are determined, and the multi-component molecular models of four rejuvenators are established. Moreover, their reliability is validated by the experimental results regarding the density values and glass transition temperature T_g ranking.

(3) From the MD simulations outputs, there is a significant difference in the energetic indices, cohesive energy density CED, solubility parameter δ, volumetric parameters, dynamic behaviors, structural indicators, expansion coefficient (α and β), and isobaric heat capacity (C_p) between the multi-component models of four rejuvenators.

(4) The order of density, CED, and δ is the same as AO > BO > NO > EO, while the fractional free volume ranking is EO > BO > NO > AO. The AO model exhibits the highest potential, valence, and total energies, while the BO shows the minimum non-bond and van der Waals energies. The relative concentration results display that the multi-component molecular model of EO and AO is the most homogeneous and uneven, respectively.

(5) The unexpected values of diffusion coefficient D, viscosity, α, β, and C_p manifest that the multi-component molecular model of aromatic-oil based on the GC–MS method is not accurate because the polycyclic aromatic molecules with heavy weight are not detected and considered.

To eliminate the limitation of the average structures, the multi-component molecular models of various rejuvenators are proposed for the first time based on the GC–MS results. However, there is still a lot of work required to promote the applications of MD simulations in rejuvenated bitumen systems. Firstly, the average models of these rejuvenators should be determined based on a series of chemical tests, and the corresponding MD simulation outputs will be compared with the results of multi-component models herein to observe the difference and provide the selection basis for the next-step MD simulations on rejuvenated bitumen. Secondly, a new chemical separation and detection method will be chosen to measure the chemical components distribution of polycyclic aromatic molecules in an aromatic-oil rejuvenator. Lastly, more chemo-physical tests should be conducted to verify the MD simulation results, and the molecular models of these rejuvenators will be further optimized.

CRediT authorship contribution statement

Shisong Ren: Methodology, Investigation, Formal analysis, Writing – original draft, Writing – review & editing. **Xueyan Liu:** Supervision, Writing – review & editing. **Sandra Erkens:** Methodology, Supervision. **Peng Lin:** Resources, Methodology, Supervision. **Yangming Gao:** Methodology, Supervision.

Declaration of Competing Interest

The authors declare that they have no known competing financial interests or personal relationships that could have appeared to influence the work reported in this paper.

Acknowledgements

The first author would thank the China Scholarship Council for the funding support (CSC, No. 201906450025).

Appendix A. Supplementary data

Supplementary data to this article can be found online at https://doi.org/10.1016/j.molliq.2022.119463.

References

[1] M. Hu, J. Ma, D. Sun, S. Ling, T. Lu, H. Ni, Understanding the aging depth gradient distribution of high viscosity modified asphalt under the effect of solar radiation and diffuse oxygen, ACS Sustainable Chemistry & Engineering. 9 (45) (2021) 15175–15189.
[2] H. Haghshenas, Chemical-physical-mechanical characterization of aging and restoration of asphaltic materials in different length scales, Dept. of Civil and Environmental Engineering, Univ. of Nebraska-Lincoln, 2018, Ph.D. dissertation.
[3] M. Guo, M. Liang, Y. Fu, A. Sreeram, A. Bhasin, Average molecular structure models of unaged asphalt binder fractions, Materials and Structures. 54 (2021) 173, https://doi.org/10.1617/s11527-021-01754-2.
[4] J. Liu, Z. Wang, R. Luo, G. Bian, Q. Liang, F. Yan, Changes of components and rheological properties of bitumen under dynamic thermal aging, Construction and Building Materials. 3030 (2021) 124501.
[5] X. Lu, H. Soenen, P. Sjovall, G. Pipintakos, Analysis of asphaltenes and maltenes before and after long-term aging of bitumen, Fuel. 304 (2021) 121426.
[6] Ren S., Liu X., Lin P., Jing R., Erkens S. Toward the long-term aging influence and novel reaction kinetics models of bitumen. International Journal of Pavement Engineering. 2022, https://doi.org/10/1080/10298436.2021.2024188.
[7] S. Ren, X. Liu, P. Lin, S. Erkens, Y. Xiao, Chemo-physical characterization and molecular dynamics simulation of long-term aging behaviors of bitumen, Construction and Building Materials. 302 (2021) 124437.

[8] G. Xu, H. Wang, Molecular dynamics study of oxidative aging effect on asphalt binder properties, Fuel. 188 (2017) 1–10.
[9] Y. Ding, D. Li, H. Zhang, M. Deng, X. Mao, X. Cao, Investigation of aging behavior of asphalt under multiple environmental conditions, Journal of Materials in Civil Engineering. 34 (2) (2022) 04021419.
[10] R. Jing, A. Varveri, X. Liu, A. Scarpas, S. Erkens, Rheological, fatigue and relaxation properties of aged bitumen, International Journal of Pavement Engineering. 21 (8) (2020) 1024–1033, https://doi.org/10.1080/10298436.2019.1654609.
[11] B. Hofko, F. Handle, L. Eberhardsteiner, M. Hospodka, R. Blab, J. Fussl, H. Grothe, Alternative approach toward the aging of asphalt binder, Transportation Research Record: Journal of the Transportation Research Board. 2505 (2015) 24–31.
[12] Mirwald J., Werkovits S., Camargo I., Maschauer D., Hofko B., Grothe H. Investigating bitumen long-term-ageing in the laboratory by spectroscopic analysis of the SARA fractions. Construction and Building Materials. 2020, 258, 119577.
[13] S. Ren, X. Liu, H. Wang, W. Fan, S. Erkens, Evaluation of rheological behaviors and anti-aging properties of recycled asphalts using low-viscosity asphalt and polymers, Journal of Cleaner Production. 253 (2020) 120048.
[14] H. Zhang, H. Zhang, H. Ding, J. Dai, Determining the sustainable component of wax-based warm mix additives for improving the cracking resistance of asphalt binders, ACS Sustainable Chemistry & Engineering. 9 (44) (2021) 15016–15026.
[15] A. Hung, E.H. Fini, Surface morphology and chemical mapping of UV-aged thin films of bitumen, ACS Sustainable Chemistry & Engineering. 8 (31) (2020) 11764–11771.
[16] K. Yan, H. Lan, Z. Duan, W. Liu, L. You, S. Wu, M. Milijkovic, Mechanical performance of asphalt rejuvenated with various vegetable oils, Construction and Building Materials. 293 (2021) 123485.
[17] X. Zhang, Y. Ning, X. Zhou, X. Xu, X. Chen, Quantifying the rejuvenation effects of soybean-oil on aged asphalt-binder using molecular dynamics simulations, Journal of Cleaner Production. 317 (2021) 128375.
[18] Gong M., Yang J., Zhang J., Zhu H., Tong T. Physical-chemical properties of aged asphalt rejuvenated by bio-oil derived from biodiesel residue. Construction and Building Materials. 2016, 105, 35-35.
[19] A. Chen, Z. Hu, M. Li, T. Bai, G. Xie, Y. Zhang, Y. Li, C. Li, Investigation on the mechanism and performance of asphalt and its mixture regenerated by waste engine oil, Construction and Building Materials. 313 (2021) 125411.
[20] F. Pahlavan, A. Rajib, S. Deng, P. Lammers, E.H. Fini, Investigation of balanced feedstocks of lipids and proteins to synthesize highly effective rejuvenators for oxidized asphalt, ACS Sustainable Chemistry & Engineering. 8 (20) (2020) 7656–7667.
[21] M. Zaumanis, R.B. Mallick, L. Poulikakos, R. Frank, Influence of six rejuvenators on the performance properties of reclaimed asphalt pavement (RAP) binder and 100% recycled asphalt mixtures, Construction and Building Materials. 71 (2014) 538–550.
[22] C. Li, A. Rajib, M. Sarker, R. Liu, E.H. Fini, J. Cai, Balancing the aromatic and ketone content of bio-oils as rejuvenators to enhance their efficacy in restoring properties of bitumen, ACS Sustainable Chemistry & Engineering. 9 (20) (2021) 6912–6922.
[23] R. Zhang, Z. You, H. Wang, X. Chen, C. Si, C. Peng, Using bio-based rejuvenator derived from waste wood to recycle old asphalt, Construction and Building Materials. 189 (2018) 568–575.
[24] H.F. Haghshenas, R. Rea, G. Reinke, M. Zaumanis, E.H. Fini, Relationship between colloidal index and chemo-rheological properties of asphalt binders modified by various recycling agents, Construction and Building Materials. 318 (2022) 126161.
[25] G. Nsengiyumva, H.F. Haghshenas, Y.R. Kim, S.R. Kommidi, Mechanical-chemical characterization of the effects of type, dosage, and treatment methods of rejuvenators in aged bituminous materials, Transportation Research Record. 2674 (3) (2020) 126–138.
[26] K. Sonibare, G. Rucker, L. Zhang, Molecular dynamics simulation on vegetable oil modified model asphalt, Construction and Building Materials. 270 (2021) 121687.
[27] Ncat, NCAT Researchers Explore Multiple User of rejuvenators asphalt technology news. 26 (NO.1 Spring) (2014) 1–16.
[28] H.F. Haghshenas, R. Rea, G. Reinke, D.F. Haghshenas, Chemical characterization of recycling agents, Journal of Materials in Civil Engineering. 32 (5) (2020) 06020005.
[29] D. Hu, X. Gu, Q. Dong, L. Lyu, B. Cui, J. Pei, Investigating the bio-rejuvenator effects on aged asphalt through exploring molecular evolution and chemical transformation of asphalt components during oxidative aging and regeneration, Journal of Cleaner Production. 329 (2021) 129711.
[30] D.D. Li, M.L. Greenfield, Chemical compositions of improved model asphalt systems for molecular simulations, Fuel. 115 (2014) 347–356.
[31] C. Chen, D. Mira, X.i. Jiang, A molecular simulation study on transport properties of FAMEs in high-pressure conditions, Fuel. 316 (2022) 123356, https://doi.org/10.1016/j.fuel.2022.123356.
[32] E.H. Fini, A. Samieadel, A. Rajib, Moisture damage and its relation to surface adsorption/desorption of rejuvenators, Industrial & Engineering Chemistry Research. 59 (30) (2020) 13414–13419.
[33] C. Bao, Y. Xu, C. Zheng, L. Nie, X. Yang, Rejuvenation effect evaluation and mechanism analysis of rejuvenators on aged asphalt using molecular simulation, Materials and Structures. 55 (2022) 52.
[34] F. Fallah, F. Khabaz, Y.R. Kim, S.R. Kommidi, H.F. Haghshenas, Molecular dynamics modeling and simulation of bituminous binder chemical aging due to variation of oxidation level and saturate-aromatic-resin-asphaltene fraction, Fuel. 237 (2019) 71–80.
[35] H. Yao, J. Liu, M.J. Xu, J., Dai Q., You Z., Discussion on molecular dynamics (MD) simulations of the asphalt materials, Advances in Colloid and Interface Science. 299 (2022) 102565.
[36] C. Yang, J. Zhang, F. Yang, M. Cheng, Y. Wang, S. Amirkahanian, S. Wu, M. Wei, J. Xie, Multi-scale performance evaluation and correlation analysis of blended asphalt and recycled asphalt mixtures incorporating high RAP content, Journal of Cleaner Production. 317 (2021) 128278.
[37] C. Bao, C. Zheng, Y. Xu, L. Nie, H. Luo, Microscopic analysis of the evolution of asphalt colloidal properties and rejuvenation behavior in aged asphalt, Journal of Cleaner Production 339 (2022) 130761, https://doi.org/10.1016/j.jclepro.2022.130761.
[38] J. Liu, Q. Liu, S. Wang, X. Zhang, C. Xiao, B. Yu, Molecular dynamics evaluation of activation mechanism of rejuvenator in reclaimed asphalt pavement (RAP) binder, Construction and Building Materials. 298 (2021) 123898.
[39] B. Cui, X. Gu, D. Hu, Q. Dong, A multiphysics evaluation of the rejuvenator effects on aged asphalt using molecular dynamics simulations, Journal of Cleaner Production 259 (2020) 120629, https://doi.org/10.1016/j.jclepro.2020.120629.
[40] Y. Kang, D. Zhou, Q. Wu, R.S. Liang, S., Liao Z., Wei N., Molecular dynamics study on the glass forming process of asphalt, Construction and Building Materials. 214 (2019) 430–440.
[41] H. Ding, H. Wang, X. Qu, A. Varveri, J. Gao, Z. You, Towards an understanding of diffusion mechanism of bio-rejuvenators in aged asphalt binder through molecular dynamics simulation, Journal of Cleaner Production. 299 (2021) 126927.
[42] G. Xu, H. Wang, Diffusion and interaction mechanism of rejuvenating agent with virgin and recycled asphalt binder: a molecular dynamics study, Molecular Simulation. 44 (17) (2018) 1433–1443.
[43] M. Xu, J. Yi, D. Feng, Y. Huang, Diffusion characteristics of asphalt rejuvenators based on molecular dynamics simulation, International Journal of Pavement Engineering. 20(5), 259 (2019) 120629.
[44] X. Han, S. Mao, S. Xu, J. Yu, Z. Cao, R. Wang, P. He, S. Zeng, Effects of reactive chain extension rejuvenation systems on the viscosity-temperature characteristics, rheological properties, and morphology of aged styrene-butadiene-styrene-modified bitumen, ACS Sustainable Chemistry & Engineering. 9 (48) (2021) 16474–16484.
[45] F. Pahlavan, A. Samieadel, S. Deng, E.H. Fini, Exploiting synergistic effects of intermolecular interactions to synthesize hybrid rejuvenators to revitalize aged asphalt, ACS Sustainable Chemistry & Engineering. 7 (8) (2019) 15514–15525.
[46] F. Pahlavan, E.H. Fini, Phenolic compounds to hinder sulfur crystallization in sulfur-extended bitumen, Resources, Conversation & Recycling. 180 (2022) 106184.
[47] Y. Xiao, B. Yan, X. Zhang, X. Chang, M. Li, Study the diffusion characteristics of rejuvenator oil in aged asphalt binder by image thresholding and GC-MS tracer analysis, Construction and Building Materials. 249 (2020) 118782.
[48] C. Hu, G. You, J. Liu, S. Du, X. Zhao, S. Wu, Study on the mechanisms of the lubricating oil antioxidants: Experimental and molecular simulation. Journal of Molecular Liquids, Journal of Molecular Liquids. 324 (2021) 115099.
[49] G. Li, Y. Tan, The construction and application of asphalt molecular model based on the quantum chemistry calculation, Fuel. 308 (2022) 122.